受入
83-8-318
高エ研図書室

EUROPEAN ORGANIZATION FOR NUCLEAR RESEARCH

CERN-EP/83-107
5 August 1983

STUDY OF MESONS PRODUCED CENTRALLY IN THE REACTION $pp \to pp + X^0$ AND $\pi^+ p \to \pi^+ p + X^0$ AT 85 GeV/c

Athens[1]-Bari[2]-Birmingham[3]-CERN[4] Collaboration

A. Palano[4,*], T.A. Armstrong[4,**], A. Apostolakis[1], A. Agelopolous[1], I.J. Bloodworth[3], A. Burns[4], J.N. Carney[3], J. Eades[4], E. Evangelista[2], B.R. French[4], B. Ghidini[2], J.B. Kinson[3], K. Knudson[4], J.-C. Lassalle[4], V. Lenti[4], W. Mitaroff[4,***], P. Papailias[1], R. Parrié[†], I.C. Print[3], E. Quercigh[4], H. Rozaki[1], H.R. Shaylor[3], M. Stassinaki[1], G. Vassiliadis[4,††], M.F. Votruba[3], G. Zito[2] and R. Zitoun[4]

ABSTRACT

Preliminary results are presented on the study of central meson production and a search for glueballs in the exclusive central meson production channels $pp \to pp + X^0$, $\pi^+ p \to \pi^+ p + X^0$ at 85 GeV/c (Experiment WA76 at CERN).

Submitted to the
International Europhysics Conference
on High-Energy Physics
Brighton, 20-27 July 1983

*) On leave from Bari University.
**) Now at Pennsylvania State University.
***) Institut für Hochenergiephysik, Vienna.
†) LPNHE, Paris.
††) On leave from Athens University.

1. INTRODUCTION

The aims of the WA76 experiment at CERN were to:

a) Study the characteristics of exclusive central meson production, and

b) Search for possible signs of glueball states in the reactions*)

$$(\pi^+/p) + p \rightarrow (\pi^+/p)_f + p_s + X^0 \qquad (1)^{*)}$$

at 85 GeV/c incident momentum.

The idea was to look in the central region where the rise in the gluon structure function at small $x_{Feynman}$ can be expected to maximize production of states coupled to glue and to look in exclusive channels where combinatorial problems are absent and therefore lower background can be expected.

The layout of the Ω' spectrometer used for this experiment is shown in Fig. 1 and it was designed in order to enhance the double exchange graphs (Double Pomeron, Regge-Pomeron, Regge-Regge), of Fig. 2, with respect to single Pomeron (diffractive) or single Regge exchange.

1.1 Trigger and apparatus

The positively charged H_1 beam (45% p, 47% π) in the West Area was incident on a 60 cm long hydrogen target and two Cerenkov counters in the beam allowed positive identification of the pions and protons.

The trigger required:

a) A fast particle defined by a hit in the counter A(54×60 cm^2) placed after Cerenkov C_2, ≥ 1 hit in a single plane of the forward MWPCs T_2 and T_3 and no hit in the beam veto counter A_0;

b) A slow particle defined by demanding one hit on any of the fourteen horizontal slabs of the Slow Proton Counter (SPC), (56×88 cm^2), and ≥ 1 hit on a single plane of the MWPCs situated on one side of the target. In addition, a hit was demanded in the side of the

---

*) In what follows the suffices f and s refer to the fastest and slowest particle in the laboratory system.

box counter (TS), surrounding the target, which was nearest the SPC.

c) In order to reduce the backward diffraction or excitation no hit was requested in the other three sides of the box TS counter which was left open at its front end to allow particles produced centrally to escape downstream.

d) To reduce the forward diffraction or excitation no hit was requested in two counters (DFC) of dimensions (30×60 cm^2) which were placed either side of the beam and just downstream of drift chamber 2 (DC2).

e) Elastic events were vetoed by demanding a forward multiplicity of ≥ 2 in the "A3" MWPC outside the beam region.

f) In addition to the above conditions (called a π trigger) a K/p trigger was imposed to select events having a negatively or positively charged kaon or proton by demanding correlated hits in the hodoscopes H_1, H_2, and H_3 along with no correlated light in the appropriate region of the multicell Cerenkov counters C_1 and C_2. The Cerenkov counters C_1 and C_2 were filled with Freon 114 and CO_2, respectively, resulting in threshold for π/K/p of 2.8/9.8/18.8 GeV/c for C_1 and 5.0/17.4/33.0 GeV/c for C_2. An air bag was placed inside C_1 in the beam region in order to reduce the multiple scattering on the fast track.

The two triggers (π and K/p) operated in parallel for most of the data taking by imposing a reduction factor (2 to 4) on the π trigger. The experiment was completed in June 1982; 8×10^6 triggers were recorded with a beam flux of 5×10^6 per pulse and 1.3×10^6 triggers were recorded with the K/p only trigger using a beam flux of 2×10^7 per pulse. The sensitivity of the experiment is of the order 2 events/nb for the π trigger and $\sim$ 10 event/nb for the K/p trigger for a centrally produced meson of mass in the region 0.5 to 2 GeV (acceptances included).

The data was processed by a modified version of the pattern recognition and geometrical reconstruction program TRIDENT [1]. Software conditions were applied to the data by asking for reconstruction of only one positive

slow track and a fast triggering track. The fraction of events satisfying the above conditions and processed for further analysis was 65%. Furthermore, the events were processed through a special program to improve the efficiency in reconstructing V^0 vertices.

2. RESULTS

The results presented below are preliminary and utilize $\sim$ 50% of the data.

Figure 3 shows a scatter plot of the pulse height recorded in the SPC versus the momentum of the track as measured in the MWPC at the side of the target. Separation of the slow π^+ from the slow proton can be made below 1 GeV/c. In the case of the fast forward particle, generally > 40 GeV/c, it was assumed that its nature was the same as the beam particle, i.e. π^+ or p. For $x_F > 0.7$ it is known[2] this assumption is correct 98% of the time. The x_F distributions for the slow and fast track selected by the trigger are shown in Fig. 4a.

2.1 The four-prong events

Amongst the various channels present in the data we have analysed the following reactions:

$$\pi^+/p + p \rightarrow (\pi^+/p)_f + p_s + (\pi^+\pi^-) \quad (2)$$

$$(K^+K^-) \quad (3)$$

$$(\bar{p}p) \quad (4)$$

$$(\pi^+\pi^-\pi^0) \ . \quad (5)$$

In order to isolate the events with no missing neutrals (4 constraint or "4c" events) we first plot the missing transverse momentum (p_t) to the four charged tracks as shown in Fig. 5a where the peak at small p_t (< 150 MeV/c) shows clear evidence for the 4c channels. When we select the sample with $|p_y| < 0.2$ GeV/c and $|p_z| < 0.12$ GeV/c and plot the missing longitudinal momentum along the beam (x-axis) we obtain the distribution shown in Fig. 5b which shows that the $p_{y,z}$ selection is selecting events in which momentum is balanced within the errors of measurement. A "4c" sample is selected by limiting $|p_x|$ to < 4 GeV/c. Events

with low momentum π^0s (< 4 GeV/c) with $|p_y| < 0.2$ GeV and $|p_z| < 0.12$ GeV are not excluded from the sample.

In order to try to separate channels (2), (3), and (4) we have used the method of Ehrlich et al.[3]. This method first sets the beam momentum vector equal to the sum of the four outgoing particle momenta and then computes the mass X of the particles in the reaction

$$\pi^+/p + p \rightarrow (\pi^+/p_f) + p_s + (X^+ + X^-) \ . \qquad (6)$$

The distribution of the mass of X squared, $m^2(X)$, after removing any events which have a track going into the Cerenkovs C_1 or C_2 which can be identified as a K, K/p or p, is shown in Fig. 6a. The peak at the π mass is evidence for the channel (2). Figure 6b shows the $m^2(X)$ distribution when events with a particle in C_1 or C_2 which can be identified as a π or p are removed. The peaks at the K mass and p mass provide evidence for the presence of channels (3) and (4) in the data. If events with a particle in C_1 and C_2 compatible with being a π, π/K or K are removed Fig. 6c results and a peak at the proton mass with little background is seen. Events where the two charged tracks do not go into C_1 or C_2 are present in all the plots. Event samples for the reactions (2), (3), and (4) were selected by making cuts on these $m^2(X)$ plots.

2.1.1 Reactions $pp \rightarrow p_f p_s(\pi^+\pi^-)$ and $\pi^+ p \rightarrow \pi^+_f p_s(\pi^+\pi^-)$

In order to understand the dynamics of the reactions we have plotted in Figs. 7a and 7b the c.m.s. rapidity (y^*) of the π^- against that of the π^+ for the reactions

$$pp \rightarrow p_f p_s(\pi^+\pi^-) \qquad (38782 \text{ events}) \qquad (2a)$$

and

$$\pi^+ p \rightarrow \pi^+_f p_s(\pi^+\pi^-) \qquad (21062 \text{ events}) \qquad (2b)$$

respectively. The presence of the forward peak in the $y^*(\pi^+)$ distribution of Fig. 7a is associated with Δ^{++} production (see Fig. 8a for the $p_f\pi^+$ effective mass distribution), which could not be vetoed out by the forward diffraction counter. However, when selecting off-line events of reaction (2a) in which the π^+ and π^- are both in the central y^* region, viz. $|y^*(\pi^+ \text{ and } \pi^-)| < 1$, no Δ^{++} is seen.

A broad accumulation at high positive $y^*_{\pi^-}$ is evident in Fig. 7b indicating the presence of diffractive contributions associated with ρ^0 and f^0 production shown in Fig. 8b where we plot the $\pi^+_f\pi^-$ mass distribution for reaction (2b).

The target box counter was much more efficient in vetoing the target excitations and this is shown in Figs. 9a and 9b where the spectra $p_s\pi^+$ and $p_s\pi^-$ for reactions (2a) and (2b) together are presented. Weak Δ^{++} signals are seen in Fig. 9a. The x_F distribution of the $\pi^+\pi^-$ system as selected by the trigger acceptance is shown in Fig. 4b.

The effective mass distributions of the $\pi^+\pi^-$ system for reactions (2a) and (2b) are shown in Figs. 10a and 10b. The ρ^0 and f^0 are evident. However, in between these two well-established meson resonances indications for another bump at a mass of 0.94 GeV is seen in both plots. If we limit the y^* of both π^+ and π^- to the central region, viz. $-1.0 < y^*(\pi^+ \text{ and } \pi^-) < 1.0$, in order to remove possible reflections of the forward Δ^{++} or ρ^0 production we obtain the distributions shown in Figs. 10c and 10d. The enhancement at 0.94 GeV remains. It is known that the $S^*(975)$ can give rise to enhancements in this mass region, and the observation of a threshold enhancement in the K^+K^- channel (see Fig. 14) suggests a description of the $\pi^+\pi^-$ mass spectrum in terms of the S^* [4]. The $\pi^+\pi^-$ mass spectrum has been fitted with an exponential background plus the ρ^0 and f^0 with masses and widths fixed at the PDT values[4]. Figure 11 shows the mass spectrum after background subtraction. The mass resolution of the $\pi^+\pi^-$ system at 950 MeV is ±10 MeV.

2.1.2 Reactions $pp \to p_f p_s(K^+K^-)$ and $\pi^+p \to \pi^+_f p_s(K^+K^-)$

The scatter plot of the K^+ and K^- rapidities in the c.m.s. for the reactions

$$pp \to p_f p_s(K^+K^-) \qquad \text{(2051 events)} \qquad (3a)$$

$$\pi^+p \to \pi^+_f p_s(K^+K^-) \qquad \text{(1132 events)} \qquad (3b)$$

is shown in Fig. 12a while the x_F distribution of the K^+K^- system is shown in Fig. 4d.

In contrast to the reactions (2a) and (2b) the kaons restrict themselves to central y^* values and there are few kaons with $|y^*| > 1$.

The pK^- spectrum shown in Fig. 13a does not show any structure while a weak $K_f^*(1420)$ is observed in the $\pi_f^+K^-$ spectrum (Fig. 13b). The above observations lead to the conclusion that the K^+K^- system is mostly produced centrally.

The K^+K^- mass spectrum summed over the two reactions (3a) and (3b) is shown in Fig. 14 and it is dominated by a threshold enhancement containing a small contribution from ϕ; some indication of $f'((1520)$ is also available.

2.1.3 Reactions $pp \to p_f p_s(p\bar{p})$ and $\pi^+p \to \pi_f p_s(p\bar{p})$

The scatter plot of the p and $\bar{p}$ rapidities in the c.m.s. for the reactions

$$pp \to p_f p_s(p\bar{p}) \qquad \text{(1288 events)} \qquad (4a)$$

$$\pi^+p \to \pi_f^+ p_s(p\bar{p}) \qquad \text{(537 events)} \qquad (4b)$$

is shown in Fig. 12b, while the $\bar{p}p$ system x_F distribution can be seen in Fig. 4e. As in the case of the K^+K^- channels the $y^*(p)$ and $y^*(\bar{p})$ distributions are concentrated around $y^* = 0$ indicating a central production of the $\bar{p}p$ system.

The $\bar{p}p$ effective mass distribution is shown in Fig. 15.

2.1.4 Reactions $pp \to pp(\pi^+\pi^-\pi^0)$ and $\pi^+p \to \pi^+p(\pi^+\pi^-\pi^0)$

The momentum balancing "4c" events were first removed from the total four-prong sample and the missing mass squared $[MM^2(X^0)]$ to the four charged prongs, assuming the presence of the reactions $pp \to p_f p_s \pi^+\pi^- X^0$ and $\pi^+p \to$ $\to \pi_f^+ p_s \pi^+\pi^- X^0$, was plotted and is shown in Fig. 16. A clear peak is seen at the π^0 mass above a considerable background. Selecting the events in the π^0 peak $[-0.2 < MM^2(X^0) < 0.3\ GeV^2]$ provides a sample of events containing the reactions

$$pp \to p_f p_s(\pi^+\pi^-\pi^0) \qquad (47626 \text{ events}) \qquad (5a)$$

and

$$\pi^+ p \to \pi^+_f p_s(\pi^+\pi^-\pi^0) \qquad (18807 \text{ events}) \ . \qquad (5b)$$

The $\pi^+\pi^-\pi^0$ effective mass distribution is shown in Fig. 17a and with a selection $|y^*(\pi^+, \pi^- \text{ and } \pi^0)| < 1.2$ is shown in Fig. 17b. This y^* selection, as with channels (2a) and (2b), removes events with forward Δ^{++} production in (5a) and ρ^0/f^0 production in (5b). The figure shows evidence for η^0 and ω^0 resonance production in the central region and shows that the resolution in the "1c" channels is sufficient for the detection of narrow states. No other clear signals are seen. The x_F distribution for the three-pion system is shown in Fig. 18a.

2.2 The four prong + V^0 events

After selecting events in which momentum is balanced (potential "4c" events) the mass distribution for the V^0s in the region of the K^0 mass is shown in Fig. 19. A clear peak at the K^0 mass is seen with little background. The width of the peak is $\sigma = \pm 6$ MeV.

The K^0 was selected between the limits $0.485 < m(\pi^+\pi^-) < 0.51$ GeV and these events were then assumed to be due to the channels

$$pp \to p_f p_s(K^0_1 K^{\pm}\pi^{\mp}) \qquad (1306 \text{ events}) \qquad (7)$$

and

$$\pi^+ p \to \pi^+_f p_s(K^0_1 K^{\pm}\pi^{\mp}) \qquad (705 \text{ events}) \ . \qquad (8)$$

Reactions (7) and (8) were selected by using the Cerenkov information and requiring $|\Delta|$ to be < 1.5 GeV^2 [Δ = missing mass squared to $(\pi^+/p)_f$ and p_s - mass squared of $(K^0_1 K^{\pm}\pi^{\mp})$]. In the case where one of the charged particles in brackets went into the Cerenkov C_1 or C_2 the resulting mass identification was used to antiselect the wrong combination otherwise the two-fold ambiguity on the nature of the charged particles remained. Reaction (7) shows a weak Δ^{++} production in the $p\pi^+$ combination which is removed by requiring $m(p\pi^+) > 1.28$ GeV.

The $K_1^0K^{\pm}\pi^{\mp}$ effective mass distributions for reactions (7), (8) and their sum are shown in Figs. 20a, b, and c. Clear signals are seen at the masses of the D^0 and E^0 mesons above a relatively low background. A fit to the spectrum with two Breit-Wigners and a polynomial background parametrization, without taking out the resolution, yields masses and widths for the D^0 and E^0 of

$$M(D^0) = 1285 \pm 2 \text{ MeV} \qquad \Gamma(D^0) = 26 \pm 5 \text{ MeV}$$

$$M(E^0) = 1432 \pm 3 \text{ MeV} \qquad \Gamma(E^0) = 58 \pm 9 \text{ MeV} .$$

No other peaks are observable in the $K_1^0K^{\pm}\pi^{\mp}$ mass spectrum.

The x_F distribution of the $K_1^0K^{\pm}\pi^{\mp}$ system is shown in Fig. 18b.

2.3 The six-prong events

Among the six-prong events we have isolated, in a manner similar to the four-prong events, the channels

$$\pi^+/p + p \to (\pi^+/p)_f p_s(2\pi^+2\pi^-) \qquad \text{(18148 events)} \qquad (9)$$

and

$$\pi^+/p + p \to (\pi/p)_f p_s(2\pi^+2\pi^-\pi^0) \qquad \text{(34428 events)} \qquad (10)$$

2.3.1 The reactions $pp \to p_f p_s(2\pi^+2\pi^-)$ and $\pi^+p \to \pi^+_f p_s(2\pi^+2\pi^-)$

As usual the Δ^{++}_f is seen in the mass spectrum of the $p_f\pi^+$ combination and the ρ^0_f in the $\pi^+_f\pi^-$ combination. These peaks disappear when we limit the $(2\pi^+2\pi^-)$ system to the central region by demanding that the $|y^*(\pi^+)|$ and $|y^*(\pi^-)|$ of the two π^+ and two π^- are all < 1.5. Figure 21a shows the total $2\pi^+2\pi^-$ effective mass spectrum and Fig. 21b the same spectrum with the y^* cut on the π's. A narrow peak is seen at the D^0 mass of 1.28 GeV and is probably the 4π decay mode of the D^0. The x_F distribution of the 4π system is shown in Fig. 18c.

2.3.2 The reactions $pp \to p_f p_s(2\pi^+2\pi^-\pi^0)$ and $\pi^+p \to \pi^+_f p_s(2\pi^+2\pi^-\pi^0)$

In these channels we have looked for the $\eta^0\pi^+\pi^-$ decay modes of the D^0 and E^0 mesons which were seen in the $K_1^0K^{\pm}\pi^{\mp}$ final state in reactions (7) and (8). The η^0 and ω^0 are seen as shoulders in the $\pi^+\pi^-\pi^0$ mass

mass to be in the region $0.51 \leq m(\pi^+\pi^-\pi^0) \leq 0.59$ GeV. To this $\pi^+\pi^-\pi^0$ system we have then assigned the η mass and formed the $\eta\pi^+\pi^-$ mass spectrum weighting each event by the inverse of the number of combinations selected. This yields the mass spectrum of Figs. 23a, b, where clear signals can be seen at the η' and D^0 masses but not at the E^0 mass. The same plots are shown in Figs. 23c, d, by requiring $|y^*_{\pi_i}| < 1.5$. The x_F distribution of the five-pion system is shown in Fig. 18d.

3. DISCUSSION AND CONCLUSIONS

We have performed an experiment aimed at searching for states with a relatively large gluon coupling which could therefore, due to the form of the gluon structure function, be expected to be produced preferentially in the central rapidity region.

We find:

a) Activity in the $\pi^+\pi^-$ mass spectrum around 1 GeV which may be due to the $S^*(975)$. Interpretation in terms of S^* is also favoured by the observation of a threshold enhancement in the K^+K^- mass spectrum.

b) Clear signals of D^0 and E^0 production above relatively little background. The signal to noise ratio here is larger than for D^0 and E^0 production in the exclusive production channels $\pi^- p \to (K^0_1 K^\pm \pi^\mp) n$ at 3.95 and 15 GeV/c [5,6] and $K^- p \to (K^0_1 K^\pm \pi^\mp)\Lambda$ [7] at 4.2 GeV/c.

c) No signal for the decay $E^0 \to \eta^0\pi^+\pi^-$ (or $\delta^\pm\pi^\mp$ as is often assumed in spin-parity analyses) in contrast to the $\eta^0\pi^+\pi^-$ signals for the D^0 and η' which are clearly seen.

d) A clear signal in the $2\pi^+2\pi^-$ mass spectrum at the D^0 mass.

e) The K^+K^-, $\bar{p}p$ and $K^0_1 K^\pm\pi^\mp$ systems are mainly produced centrally with little contribution in the diffractive region; this is in contrast to the $\pi^+\pi^-$ system, which together with a strong central production, shows also an accumulation of events in the diffractive region of y^*.

Summarizing, we see clear signals for the central production of S^*, D^0 and E^0 mesons with a signal to background ratio which is significantly higher than that seen in peripheral reactions[5-8] and of the same order as that seen for the E/ι in J/ψ radiative decay[9,10].

REFERENCES

1) J.-C. Lassalle et al., Nucl. Instrum. Methods 176 (1980) 371.

2) C.P. Ward et al., Nucl. Phys. B153 (1979) 299.

3) R. Ehrlich et al., Phys. Rev. Lett. 20 (1968) 686.

4) Particle Data Group, Phys. Lett. 111B (1982).

5) C. Dionisi et al., Nucl. Phys. B169 (1980) 1.

6) M.J. Corden et al., Nucl. Phys. B144 (1978) 253.

7) A. Gurtu et al., Nucl. Phys. B151 (1979) 181.

8) A.J. Pawlicki et al., Phys. Rev. D 15 (1977) 3196.

9) D.L. Scharre et al., Phys. Lett. 97B (1980) 329.

10) C. Edwards et al., Phys. Rev. Lett. 49 (1982) 259.

Figure captions

Fig. 1 : Layout of the Ω' spectrometer as used in the present experiment.

Fig. 2 : Exchange graphs contributing to the reactions produced in the present experiment.

Fig. 3 : ADC pulse height versus the momentum of the recoiling slow particle. Clear separation is evident between π^+ and p.

Fig. 4 : a) Feynman x distributions for the fast and slow particle.
b) x_F distribution for the $\pi^+\pi^-$ system for incident π^+. The dashed line represents the effect of the $y^*_{\pi_i}$ cuts applied to the data in order to select the central region as discussed in the text.
c) As (b) but with incident protons.
d) x_F distribution for the $p\bar{p}$ system.

Fig. 5 : a) Missing transverse momentum distribution for the four-prong events.
b) Missing longitudinal momentum distribution for the four-prong events after having applied p_T cuts as explained in the text.

Fig. 6 : a) m_x^2 distribution for event candidates of reactions (2a) and (2b). Events with either the positive or the negative track crossing the Cerenkov counters C_1 and C_2 identified as D, p or k/p ambiguity have been removed.
b) As in (a) but removing tracks uniquely identified as π or p.
c) As in (a) but removing tracks uniquely identified as π or K.
The arrows indicate the cuts used to select reactions (2a), (2b), (3a), (3b), (4a), and (4b).

Fig. 7 : a) $y^*(\pi^+)$ vs. $y^*(\pi^-)$ for reaction (2a).
b) $y^*(\pi^+)$ vs. $y^*(\pi^-)$ for reaction (2b).

Fig. 8 : a) $m(p_f\pi^+)$ distribution for reaction (2a).
b) $m(\pi^+_f\pi^-)$ distribution for reaction (2b).

Fig. 9 : a) $m(p_s\pi^+)$ distribution for reactions (2a) and (2b) summed together.
b) $m(p_s\pi^-)$ distribution for reactions (2a) and (2b) summed together.

Fig. 10 : a) Effective mass distribution $m(\pi^+\pi^-)$ for reaction (2a).
b) Effective mass distribution $m(\pi^+\pi^-)$ for reaction (2b).
c) $m(\pi^+\pi^-)$ for reaction (2a) after having selected $|y^*|$ of each pion to be below 1.
d) $m(\pi^+\pi^-)$ for reaction (2b) after having selected $|y^*|$ of each pion to be below 1.

Fig. 11 : $m(\pi^+\pi^-)$ after background subtraction.

Fig. 12 : a) $y^*(K^+)$ vs. $y^*(K^-)$ for reactions (3a) and (3b).
b) $y^*(p)$ vs. $y^*(\bar{p})$ for reactions (4a) and (4b).

Fig. 13 : a) Effective mass distribution p_fK^- for reaction (3a).
b) Effective mass distribution $\pi^+_fK^-$ for reaction (3b).

Fig. 14 : Effective mass distribution for the K^+K^- system.

Fig. 15 : Effective mass distribution for the $p\bar{p}$ system.

Fig. 16 : Squared missing mass to the $(\pi^+_f/p_f)p_s\pi^+\pi^-$ system after having removed the "4c" events. The arrows indicate the cuts used to select the π^0.

Fig. 17 : a) Effective mass distribution for the $\pi^+\pi^-\pi^0$ system.
b) $m(\pi^+\pi^-\pi^0)$ after having requested each of the three pions to have a |rapidity| in the centre of mass system < 1.2.

Fig. 18 : a) Feynman x distribution for the $\pi^+\pi^-\pi^0$ system. The dashed line represents the effect of the rapidity cut.
b) $x_F(K^0_1K^\pm\pi^\mp)$.
c) $x_F(\pi^+\pi^-\pi^+\pi^-)$. The dashed distribution shows the effect of the rapidity cut.
d) $x_F(\pi^+\pi^-\pi^+\pi^-\pi^0)$. The dashed line shows the effect of the rapidity cut.

Fig. 19 : Effective mass distribution $m(\pi^+\pi^-)$ for tracks belonging to a V^0 vertex. Momentum conservation is also requested in this plot.

Fig. 20 : a) $K_1^0 K^{\pm}\pi^{\mp}$ mass distribution for reaction (7); and
b) For reaction (8).
c) Reactions (7) and (8) summed.

Fig. 21 : Effective mass distribution for the 4π system in reactions (9).
a) Uncut.
b) Rapidity cuts.

Fig. 22 : Effective mass distribution $\pi^+\pi^-\pi^0$ for reactions (10) (four combinations per event).
a) Uncut.
b) With rapidity cuts.

Fig. 23 : Effective mass distribution $\eta\pi^+\pi^-$.
a) π^+ incident.
b) p incident.
c) π^+ incident and rapidity cuts.
d) p incident and rapidity cuts.

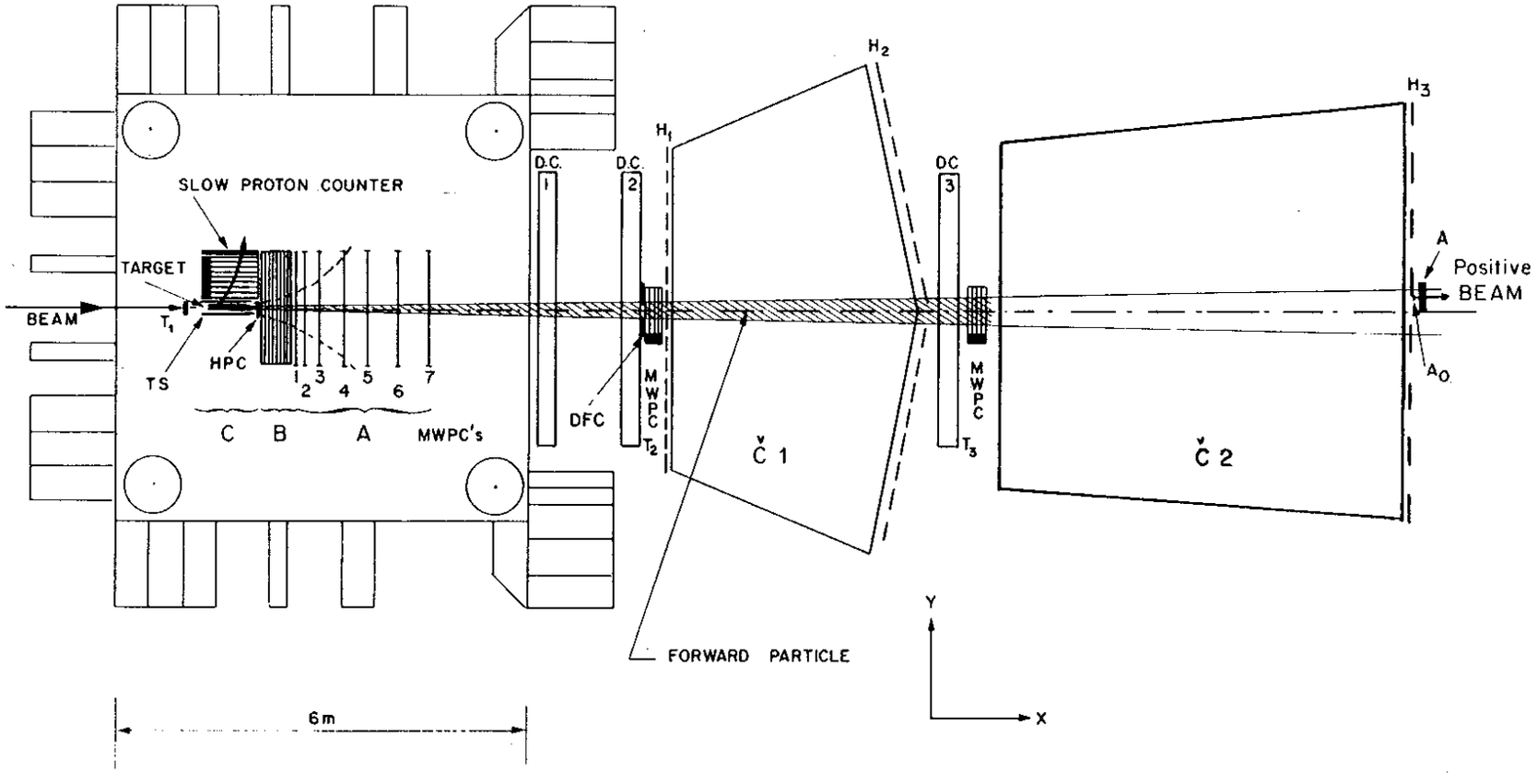

Experiment WA76: Study of the Mesons Produced Centrally in the Reaction
$pp \rightarrow pp + X^0$ and $\pi^+p \rightarrow \pi^+p + X^0$ at 85 GeV/c

Fig.1

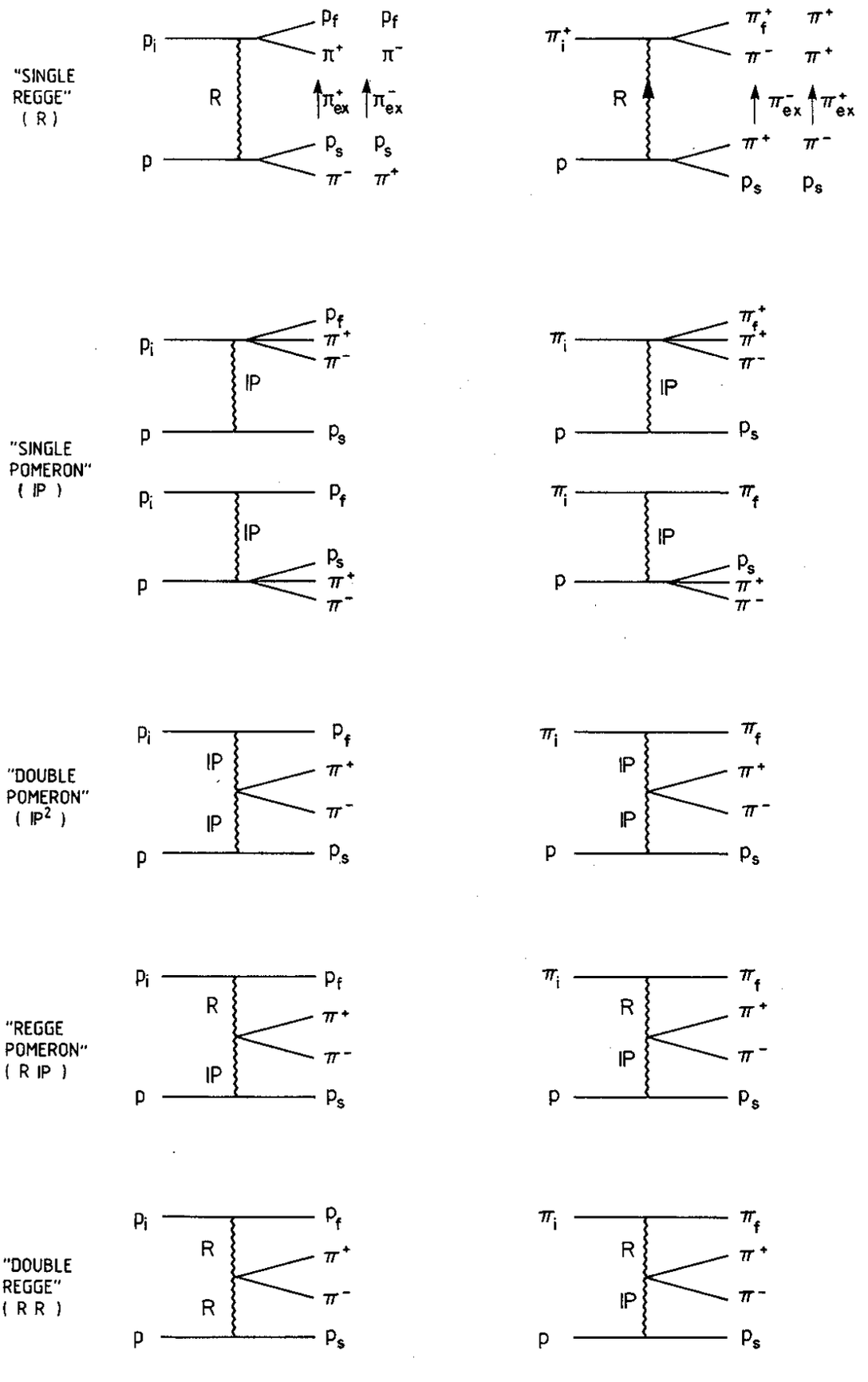
"SINGLE REGGE" (R)
"SINGLE POMERON" (IP)
"DOUBLE POMERON" (IP²)
"REGGE POMERON" (R IP)
"DOUBLE REGGE" (R R)
R
IP

Fig. 2

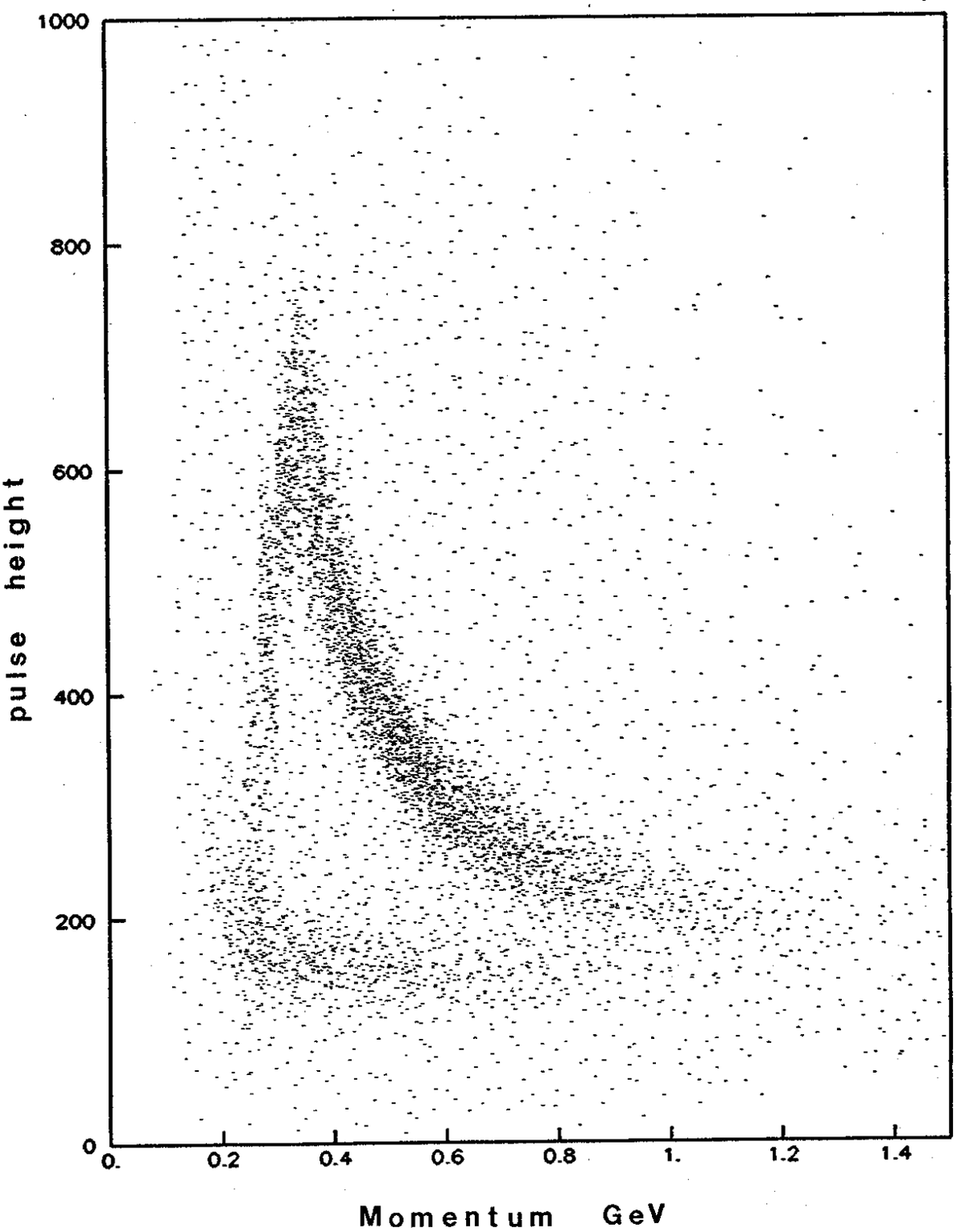
1000
800
600
400
200
0
pulse height
0.
0.2
0.4
0.6
0.8
1.
1.2
1.4
Momentum GeV

Fig. 3

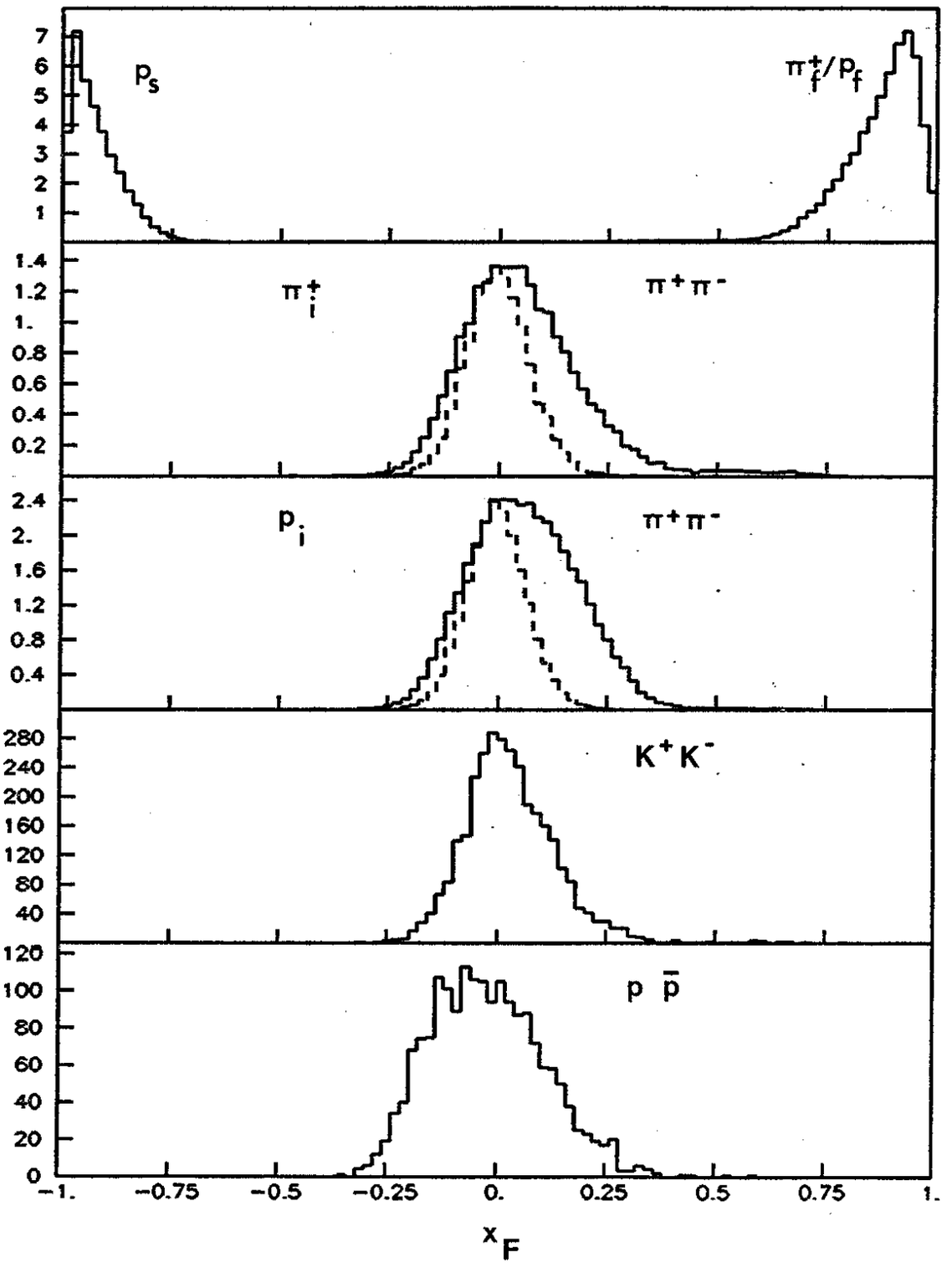

Fig. 4

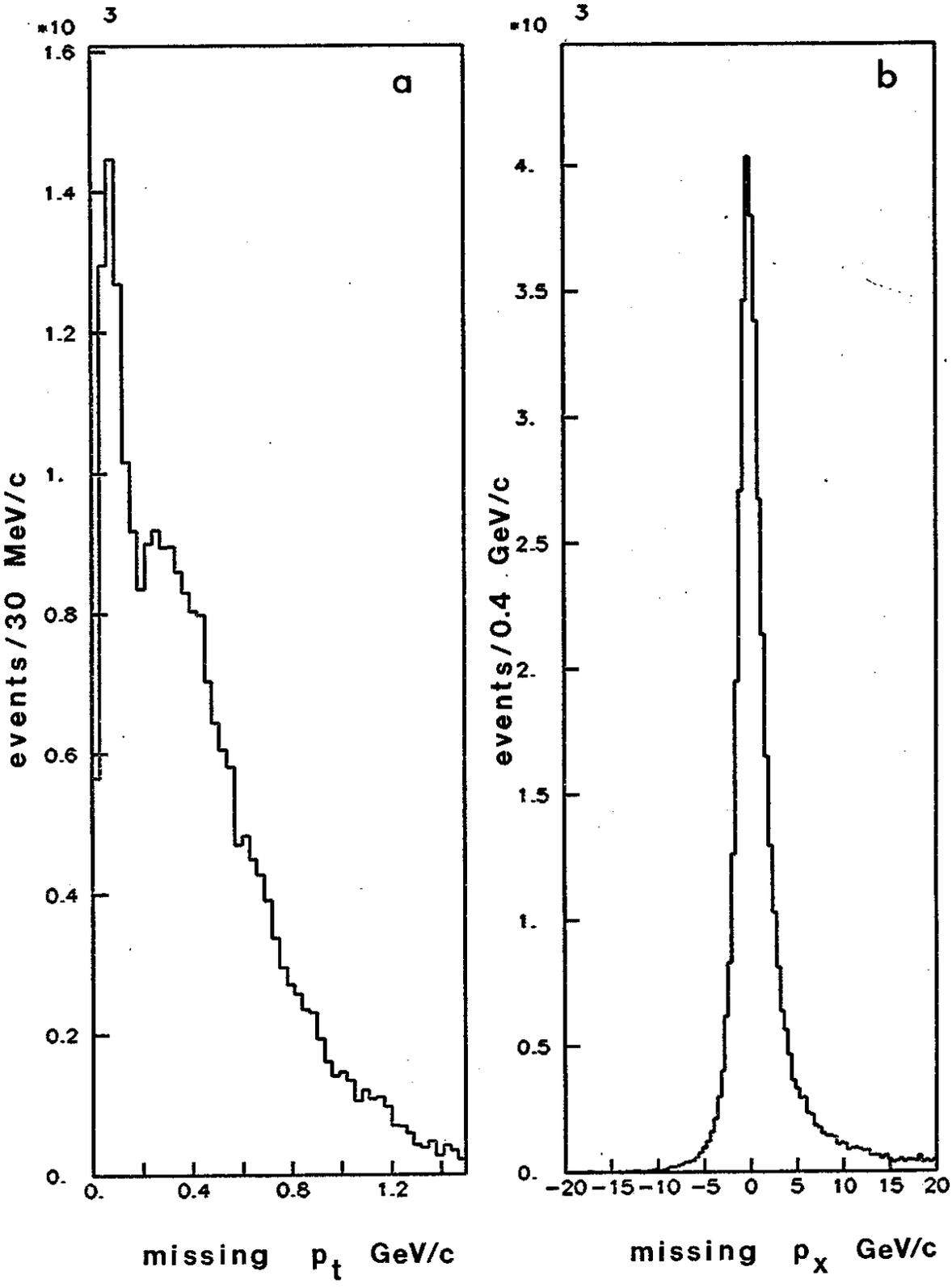
a
b
*10 3
events/30 MeV/c
events/0.4 GeV/c
missing p_t GeV/c
missing p_x GeV/c

Fig. 5

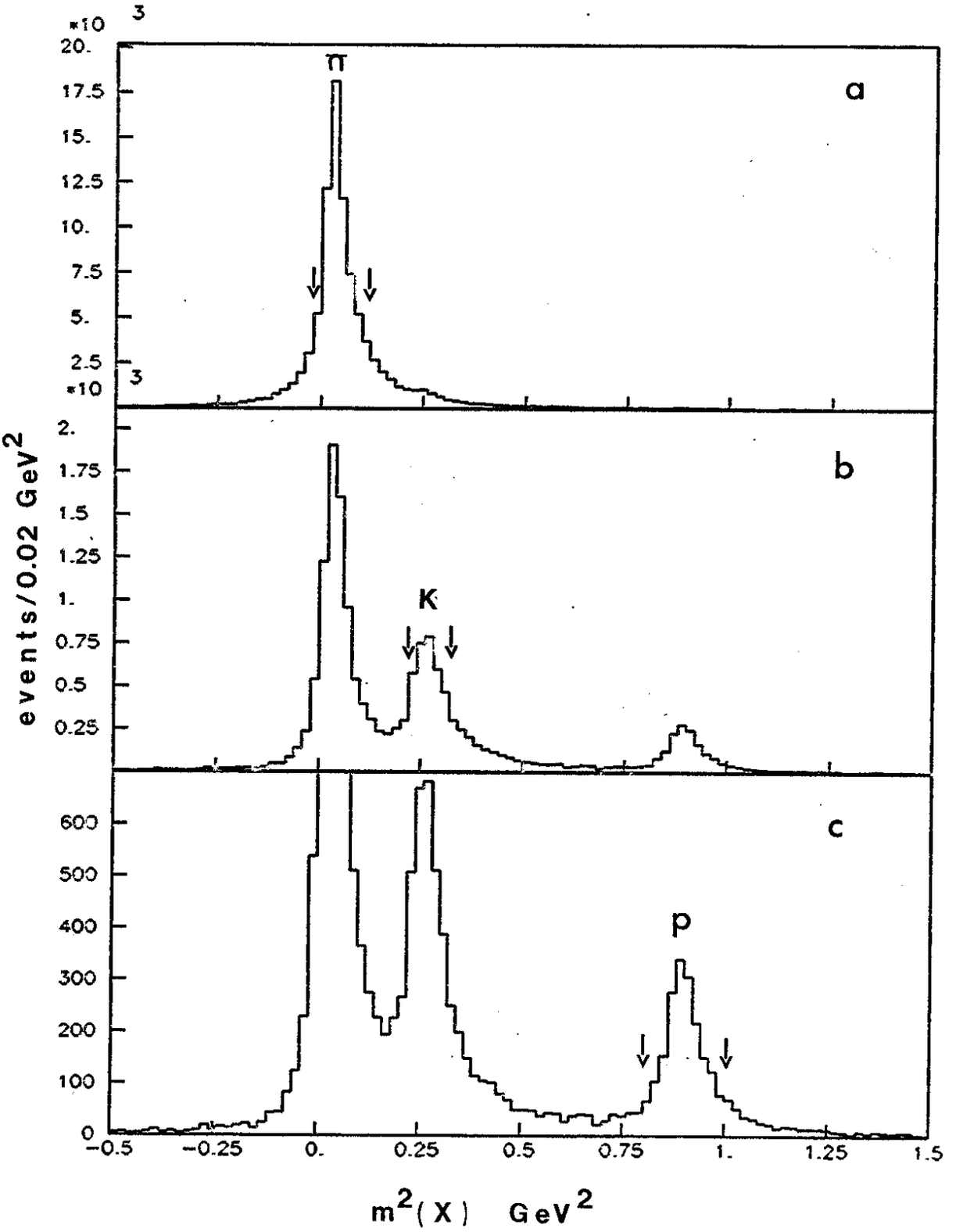
×10 3
20.
17.5
15.
12.5
10.
7.5
5.
2.5
×10 3
π
a
b
K
c
p
events/0.02 GeV²
2.
1.75
1.5
1.25
1.
0.75
0.5
0.25
600
500
400
300
200
100
0
−0.5
−0.25
0.
0.25
0.5
0.75
1.
1.25
1.5
m²(X) GeV²

Fig. 6

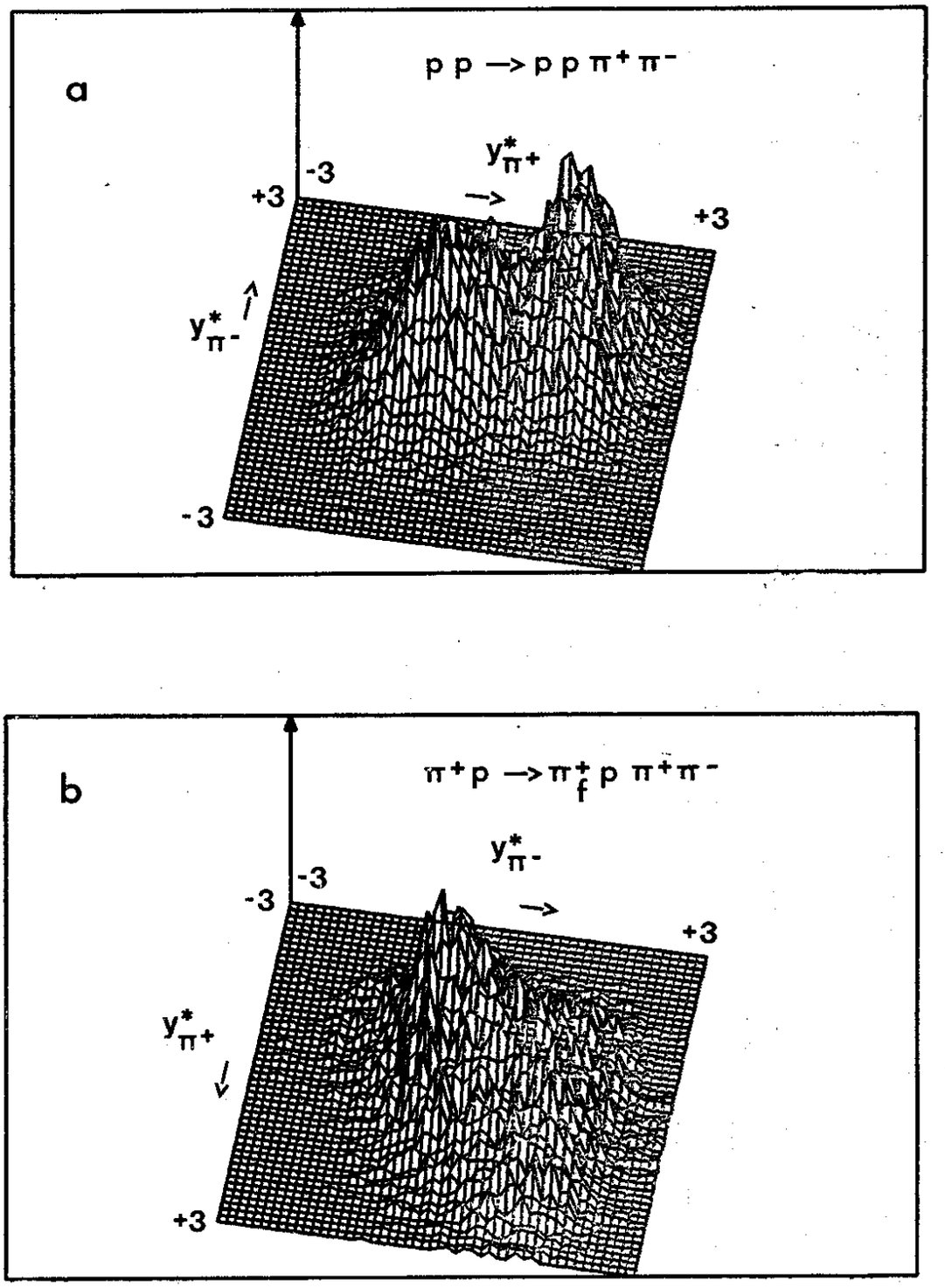

FIG. 7

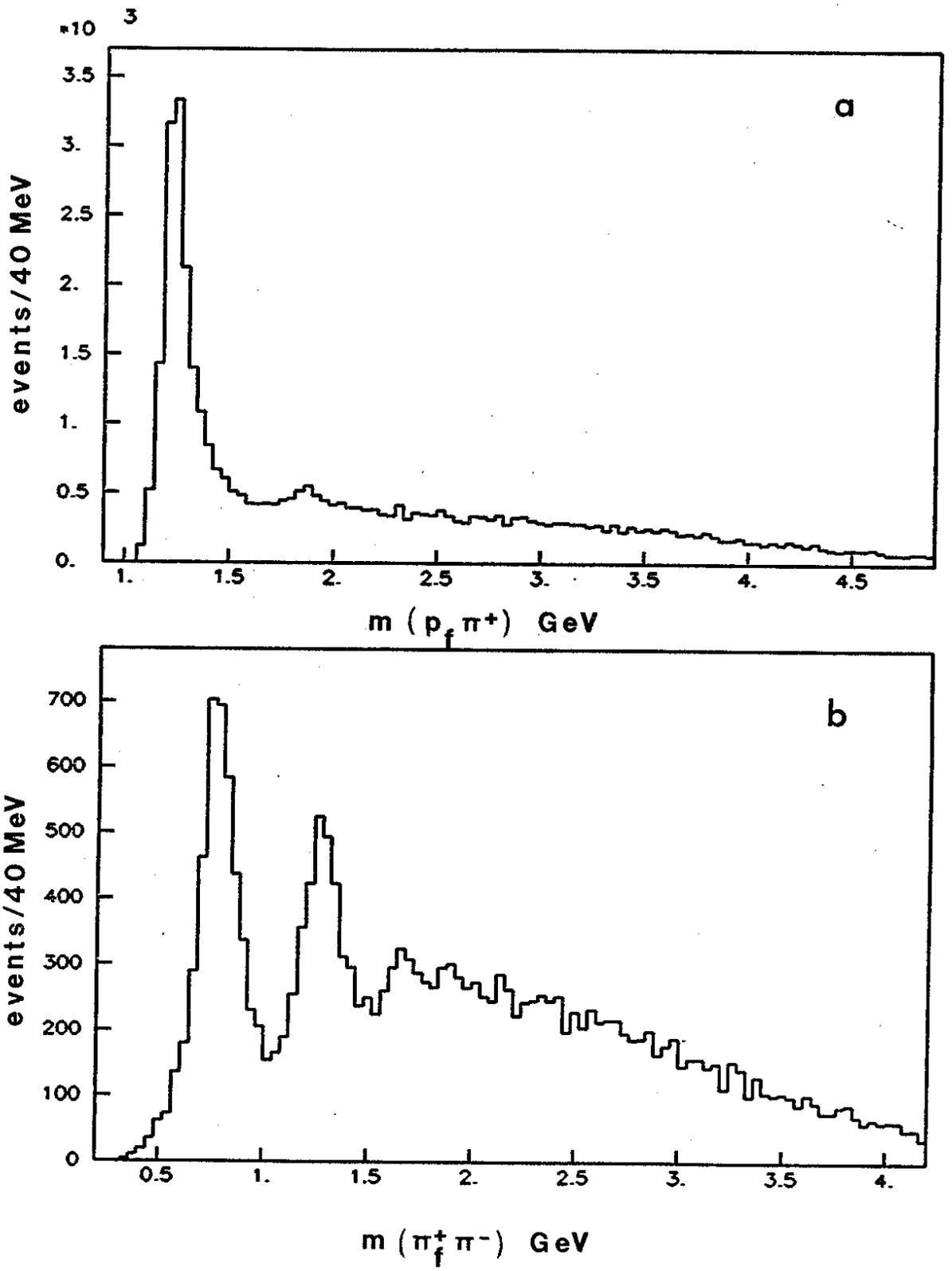
×10 3
3.5
3.
2.5
2.
1.5
1.
0.5
0.
events/40 MeV
a
1.
1.5
2.
2.5
3.
3.5
4.
4.5
m (p_f π+) GeV
700
600
500
400
300
200
100
0
events/40 MeV
b
0.5
1.
1.5
2.
2.5
3.
3.5
4.
m (π+_f π-) GeV

Fig. 8

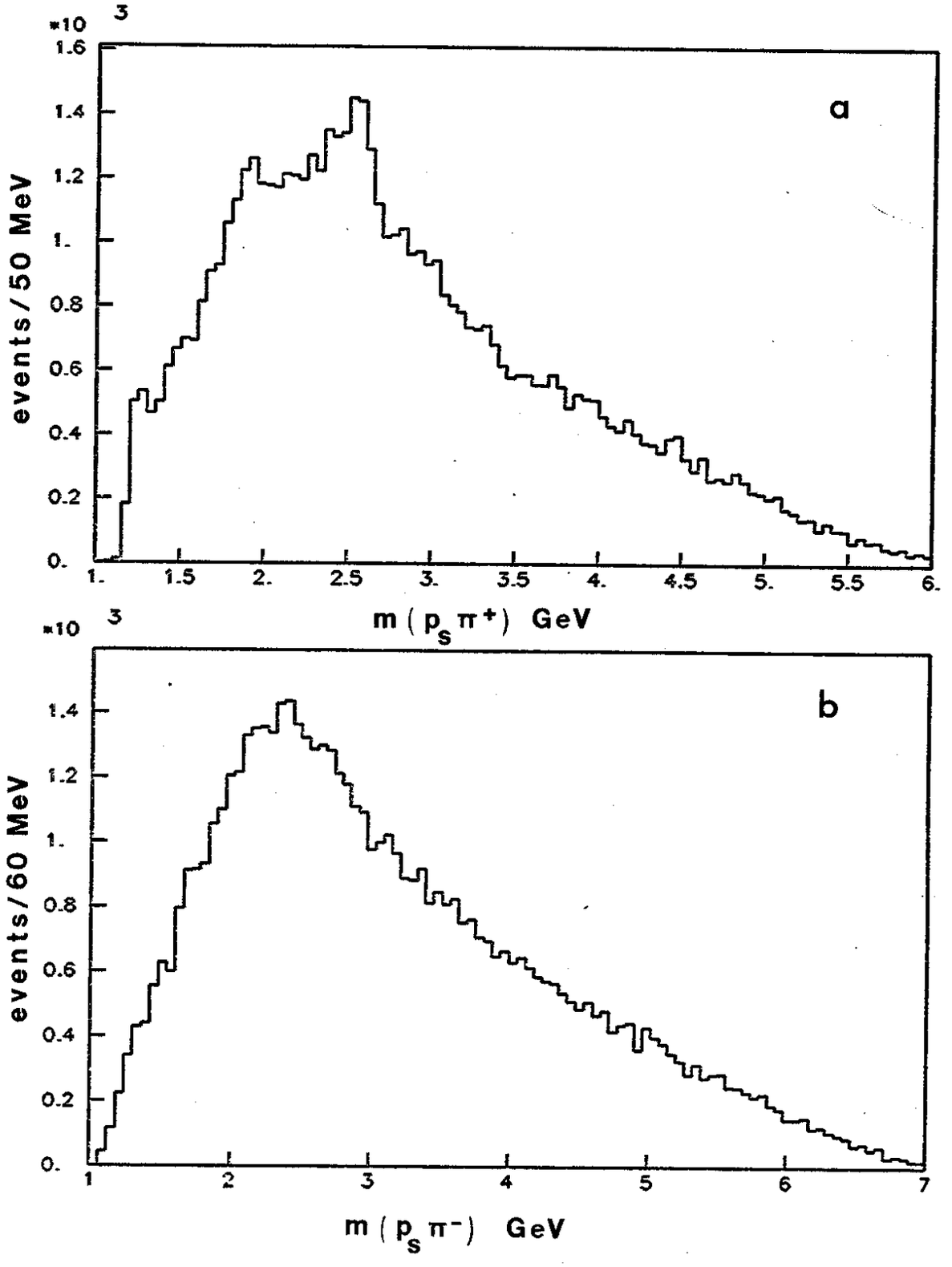
×10 3
1.6
1.4
1.2
1.
0.8
0.6
0.4
0.2
0.
events/50 MeV
a
1.
1.5
2.
2.5
3.
3.5
4.
4.5
5.
5.5
6.
m (p_s π+) GeV
×10 3
1.4
1.2
1.
0.8
0.6
0.4
0.2
0.
events/60 MeV
b
1
2
3
4
5
6
7
m (p_s π-) GeV

Fig. 9

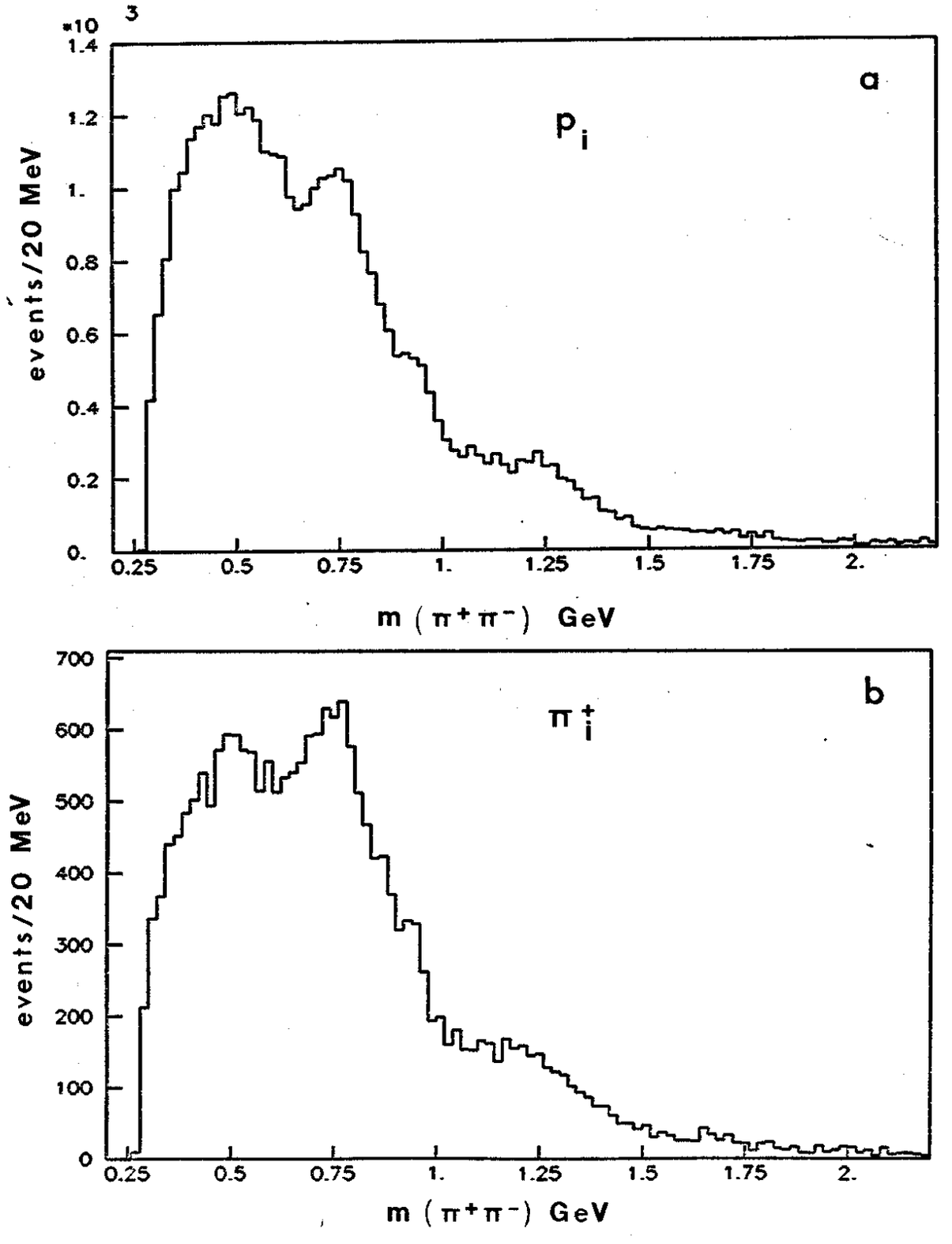

Fig.10

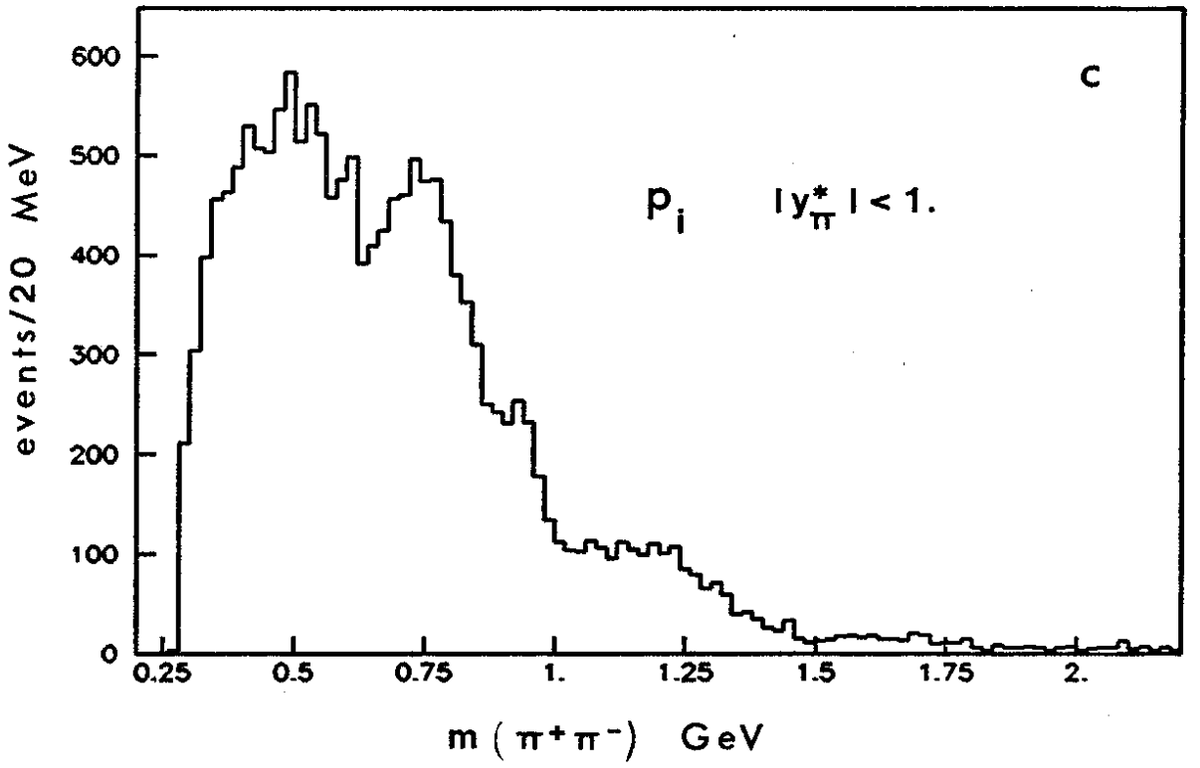
c
p_i $|y^*_\pi| < 1.$
events/20 MeV
600
500
400
300
200
100
0
0.25
0.5
0.75
1.
1.25
1.5
1.75
2.
$m(\pi^+\pi^-)$ GeV

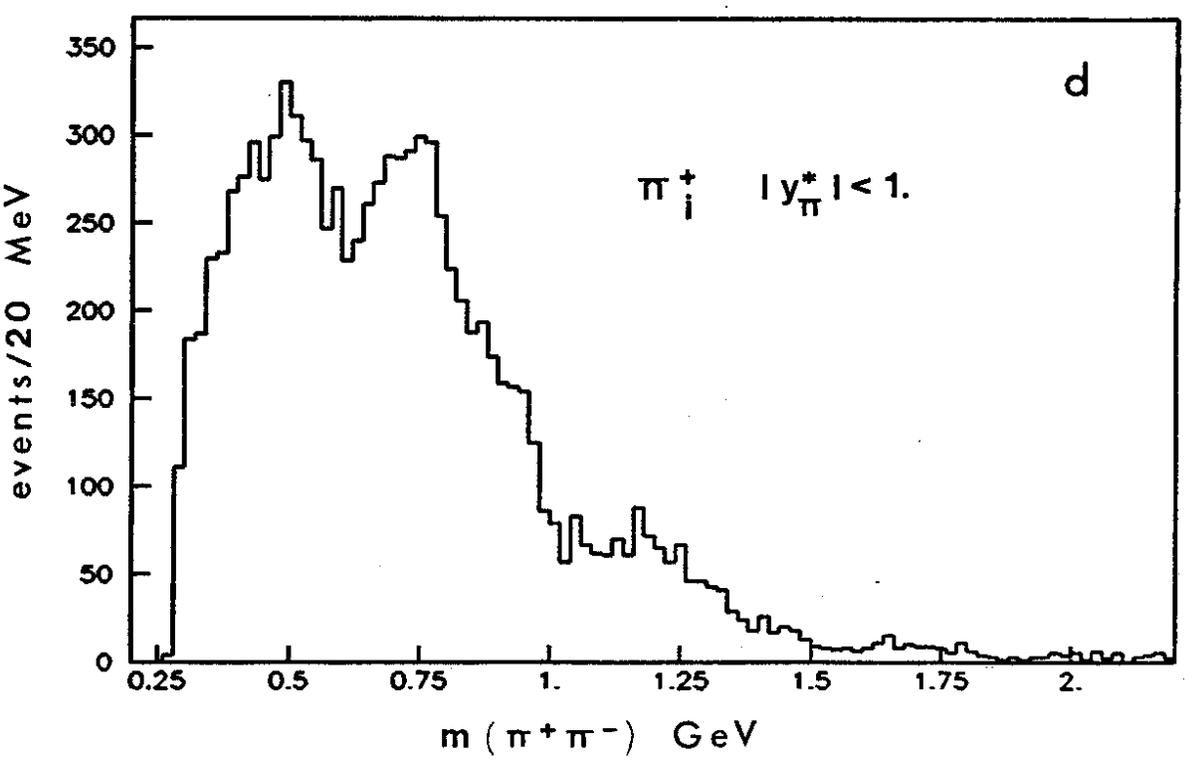
d
π^+_i $|y^*_\pi| < 1.$
events/20 MeV
350
300
250
200
150
100
50
0
0.25
0.5
0.75
1.
1.25
1.5
1.75
2.
$m(\pi^+\pi^-)$ GeV

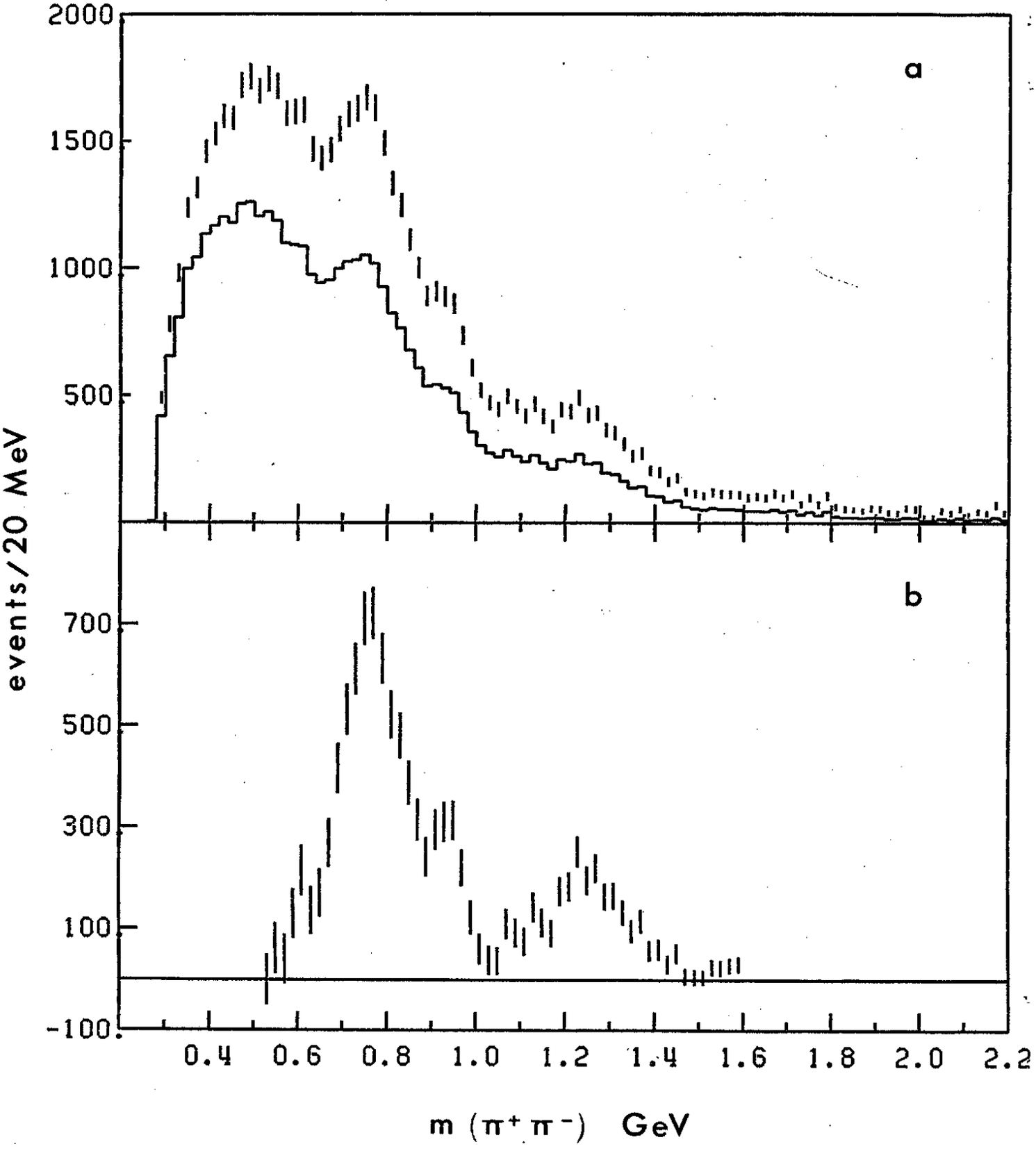
2000
1500
1000
500
a
b
700
500
300
100
-100
events/20 MeV
0.4
0.6
0.8
1.0
1.2
1.4
1.6
1.8
2.0
2.2
m (π+ π−) GeV

Fig. 11

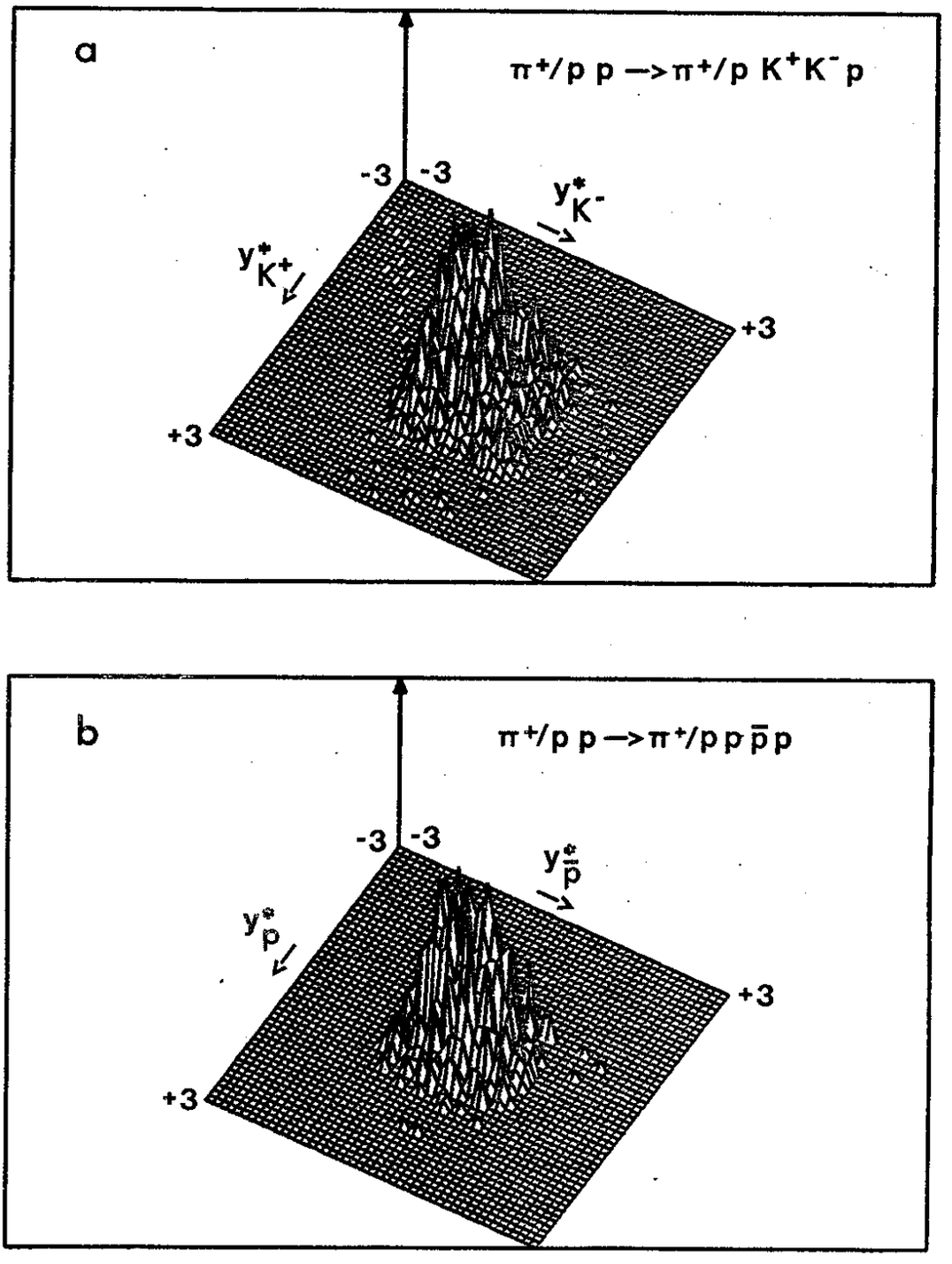
a
$\pi^+/p\ p \rightarrow \pi^+/p\ K^+K^-\ p$
-3
-3
$y^*_{K^-}$
$y^*_{K^+}$
+3
+3
b
$\pi^+/p\ p \rightarrow \pi^+/p\ p\ \bar{p}\ p$
-3
-3
$y^*_{\bar{p}}$
y^*_{p}
+3
+3

FIG. 12

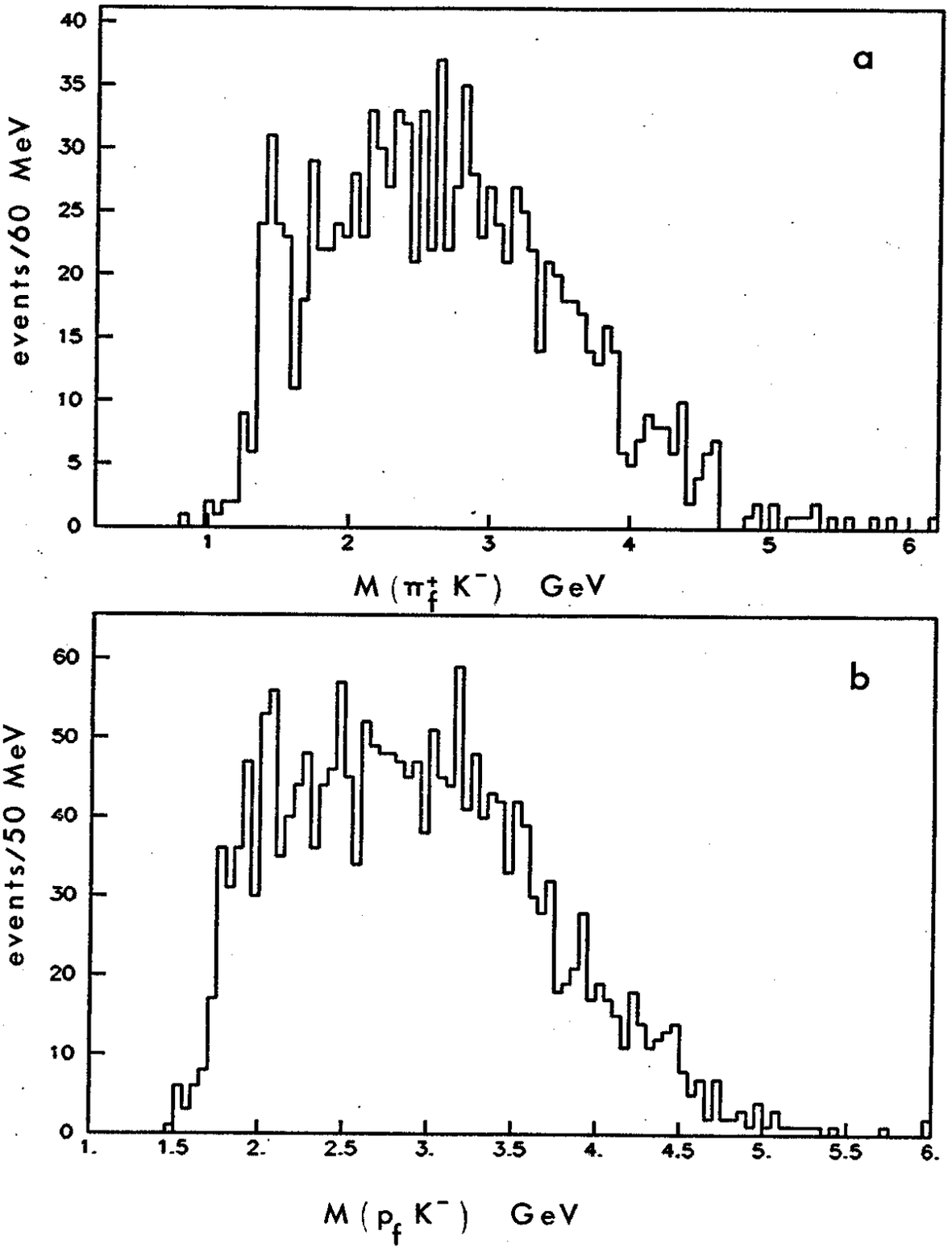

Fig. 13

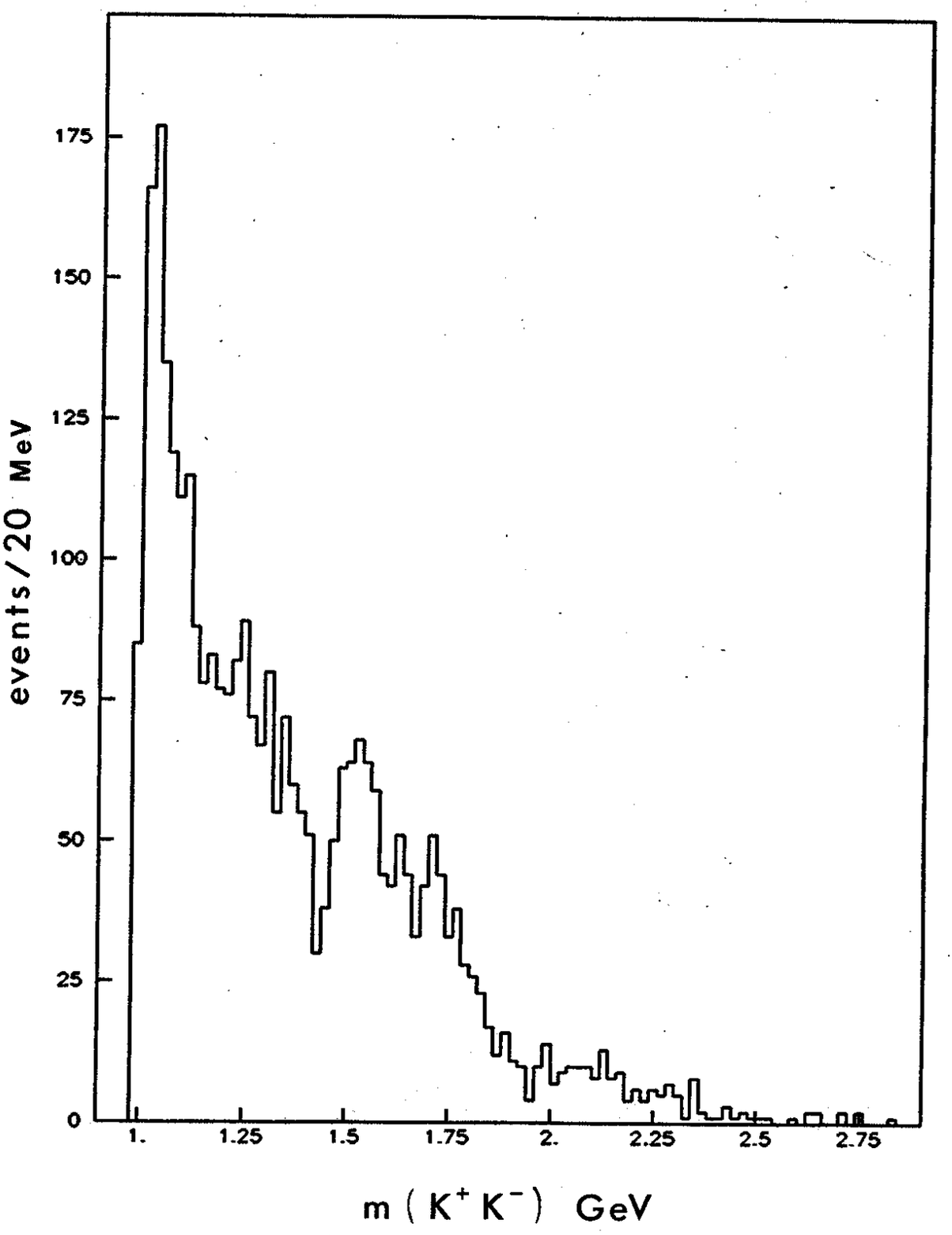
events / 20 MeV
175
150
125
100
75
50
25
0
1.
1.25
1.5
1.75
2.
2.25
2.5
2.75
m (K⁺ K⁻) GeV

Fig. 14

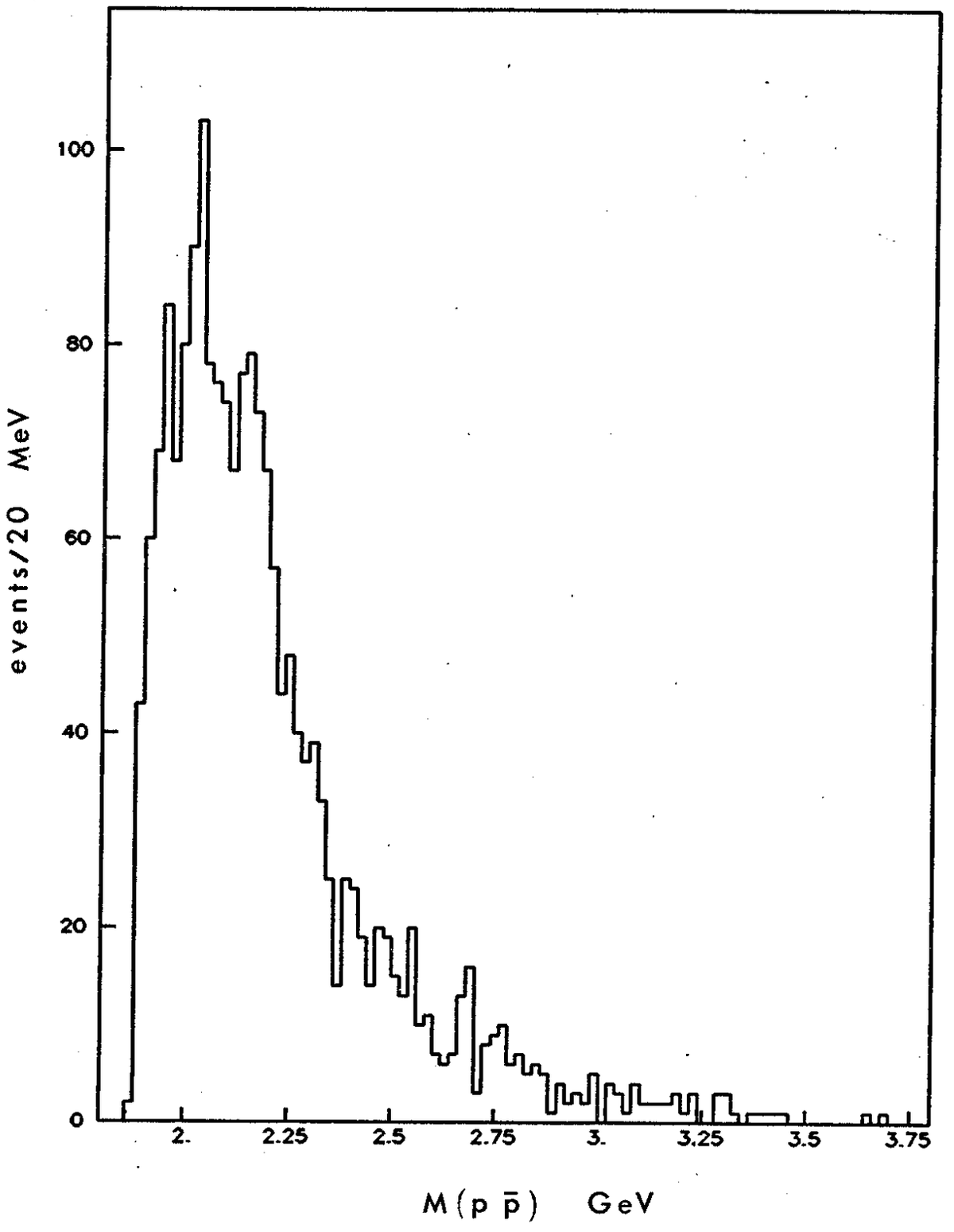

Fig. 15

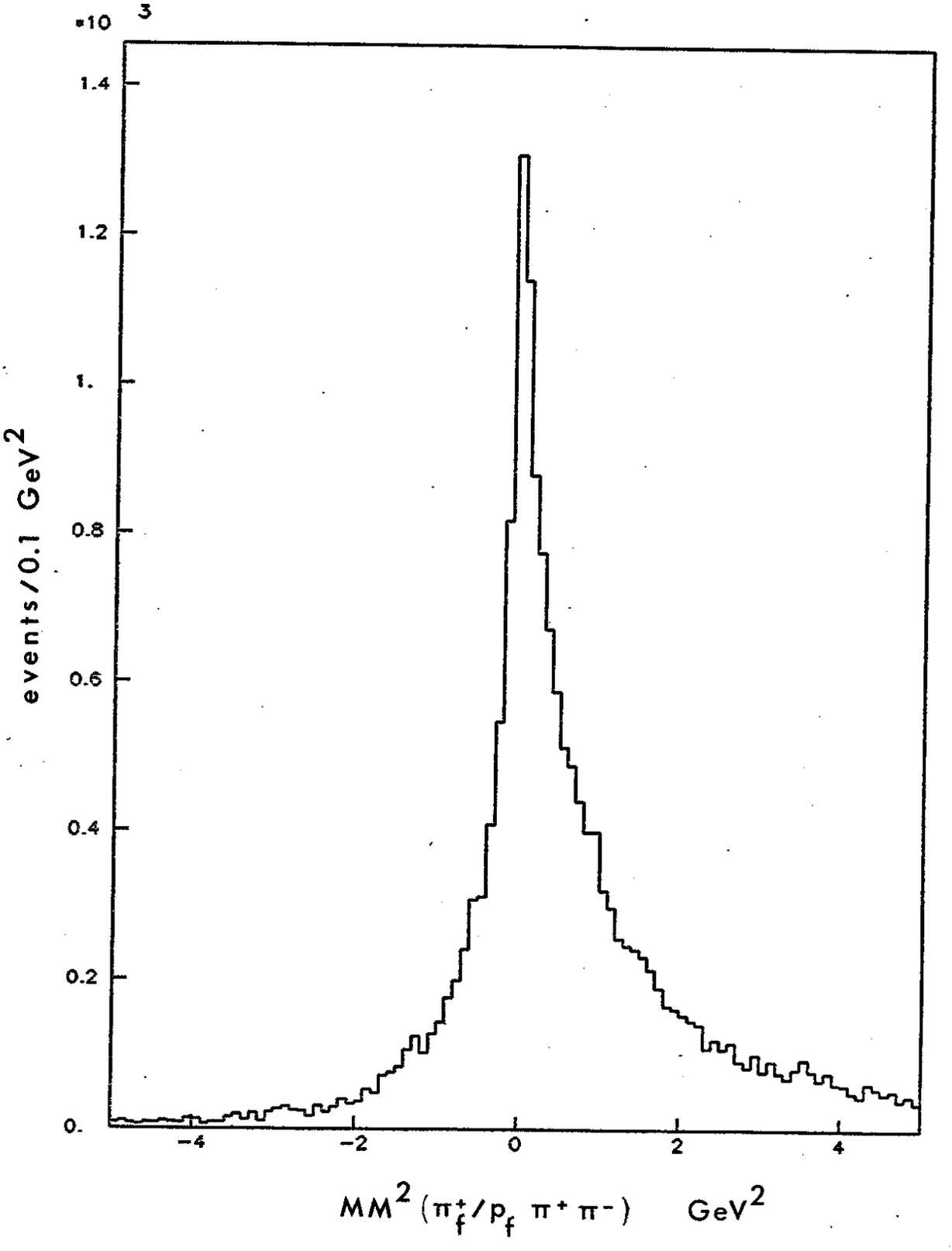
*10 3
1.4
1.2
1.
0.8
0.6
0.4
0.2
0.
events/0.1 GeV^2
-4
-2
0
2
4
MM^2 (π_f^+/p_f π^+ π^-) GeV^2

Fig. 16

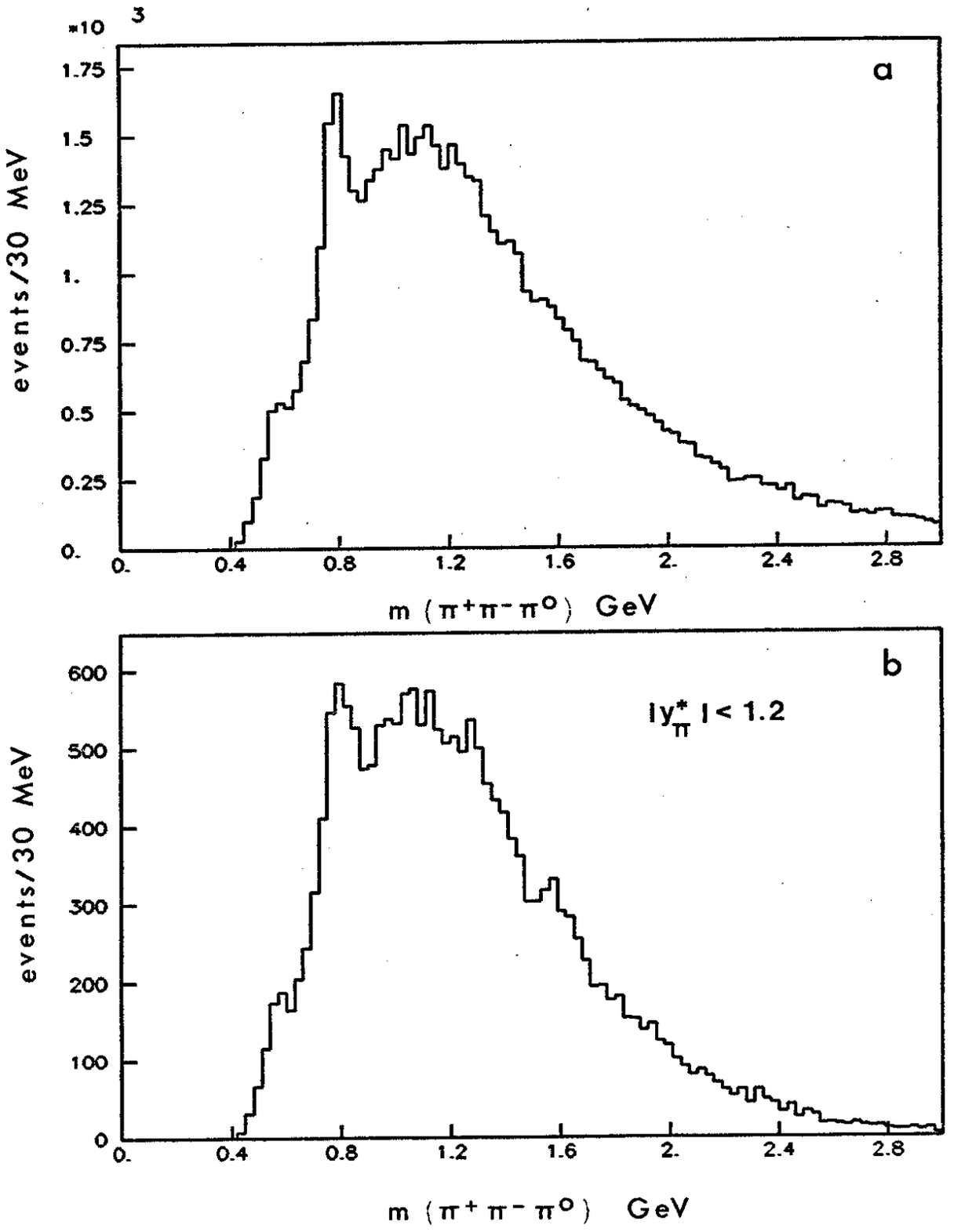
×10 3
1.75
1.5
1.25
1.
0.75
0.5
0.25
0.
events/30 MeV
a
0.
0.4
0.8
1.2
1.6
2.
2.4
2.8
m (π+π-π°) GeV
600
500
400
300
200
100
0
events/30 MeV
b
|y*π| < 1.2
0.
0.4
0.8
1.2
1.6
2.
2.4
2.8
m (π+ π- π°) GeV

Fig. 17

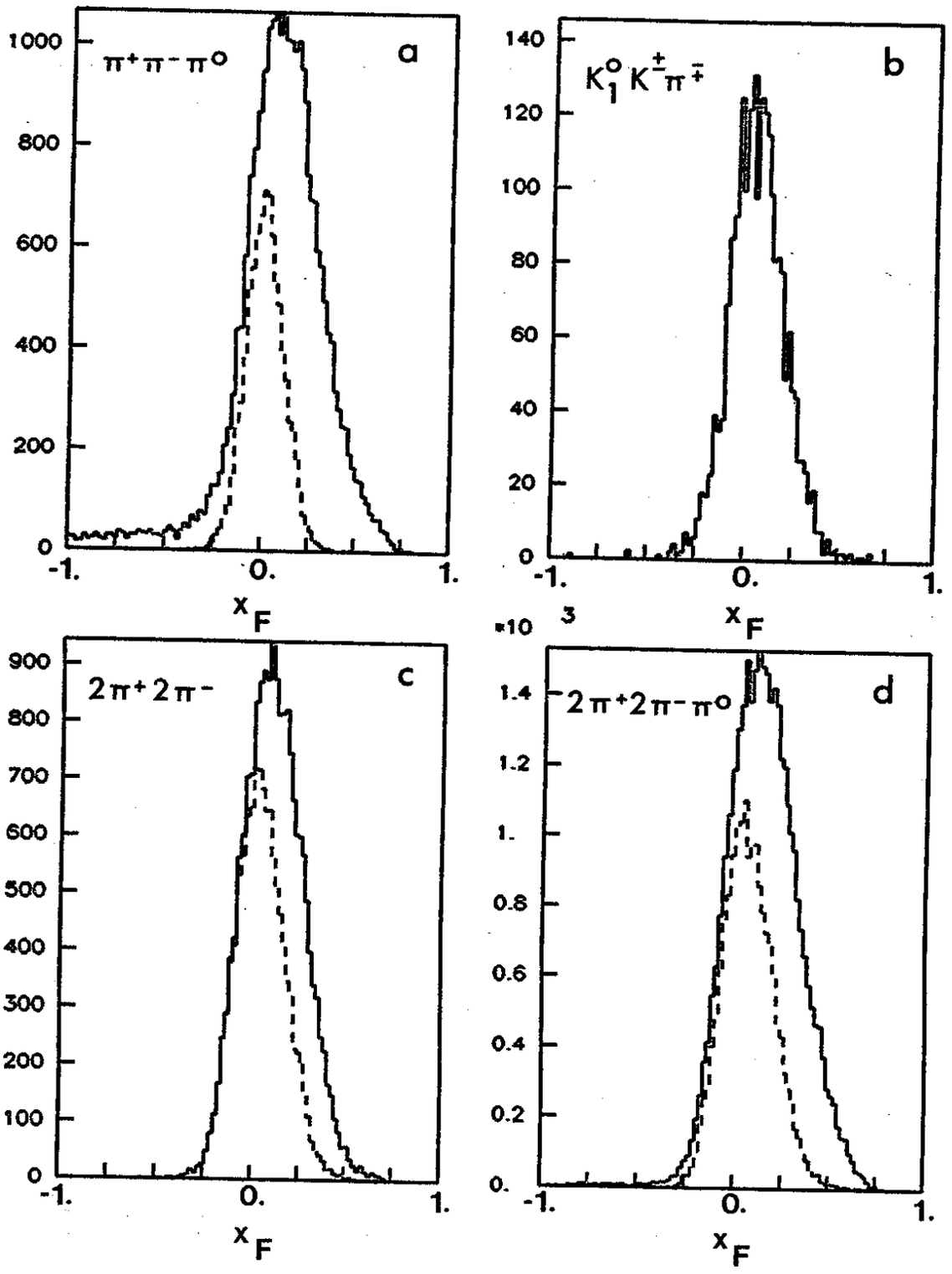
a
$\pi^+\pi^-\pi^o$
1000
800
600
400
200
0
-1.
0.
1.
x_F
b
$K_1^o K^{\pm}\pi^{\mp}$
140
120
100
80
60
40
20
0
-1.
0.
1.
x_F
c
$2\pi^+2\pi^-$
900
800
700
600
500
400
300
200
100
0
-1.
0.
1.
x_F
d
$2\pi^+2\pi^-\pi^o$
$\times 10^3$
1.4
1.2
1.
0.8
0.6
0.4
0.2
0.
-1.
0.
1.
x_F

Fig. 18

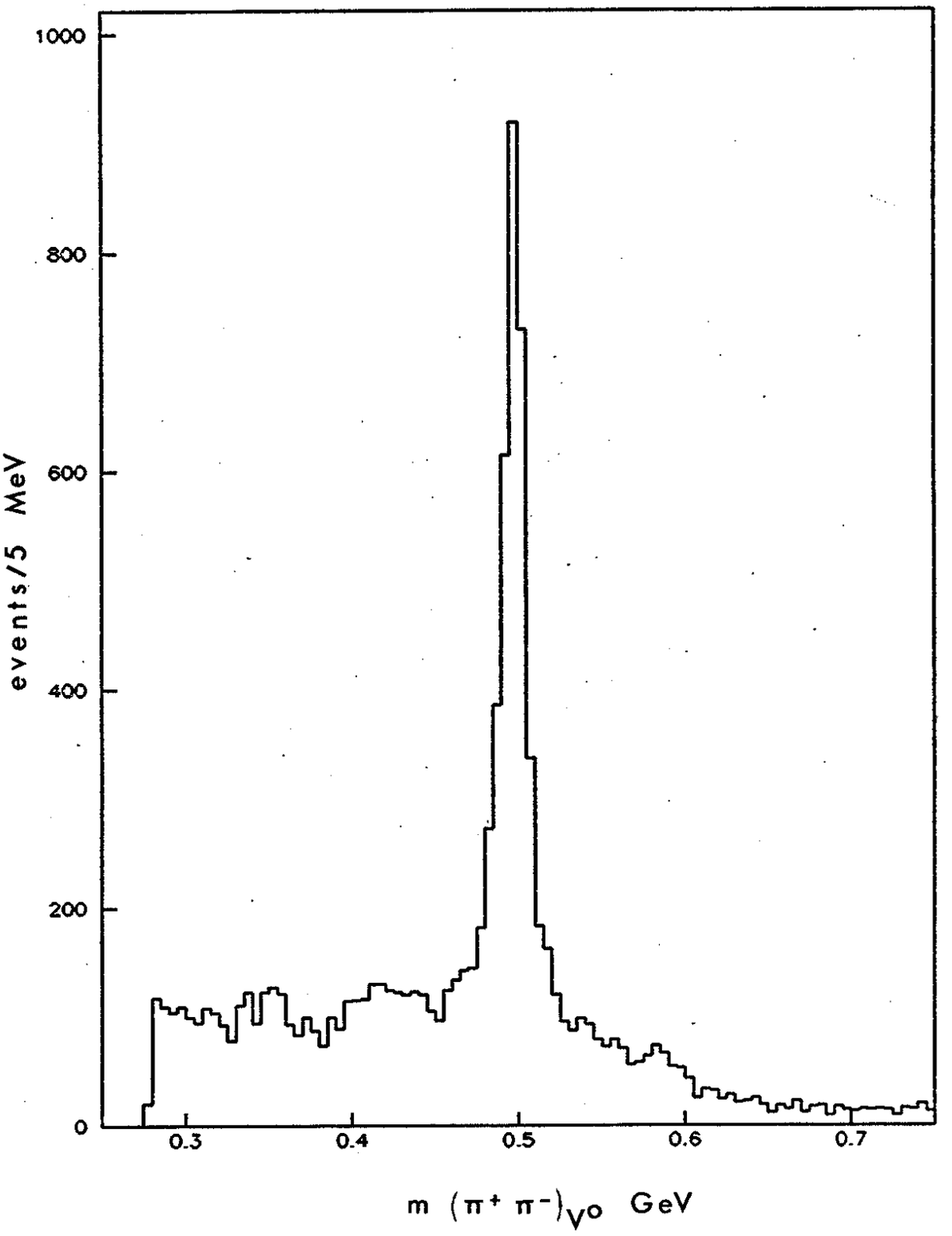

Fig. 19

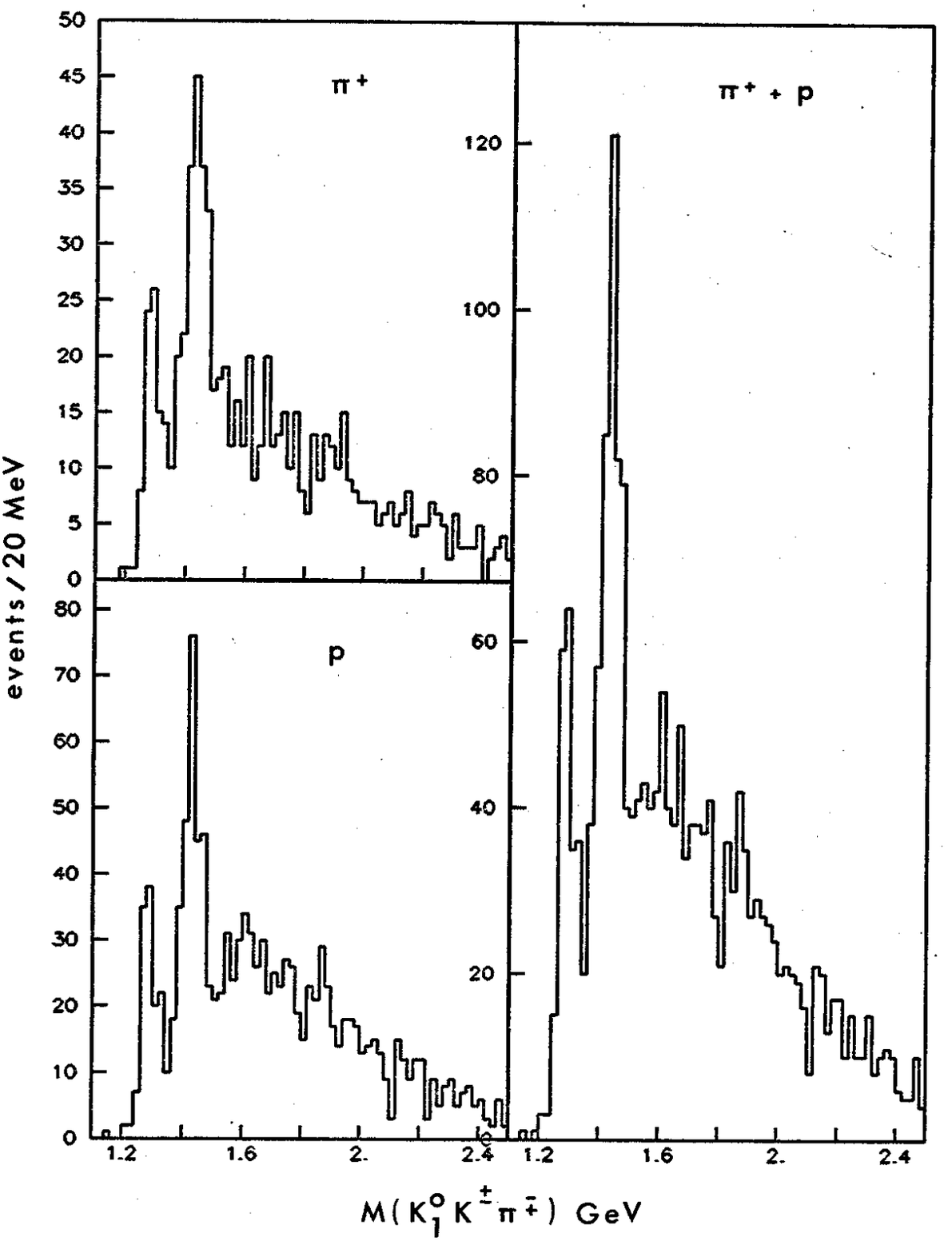

Fig. 20

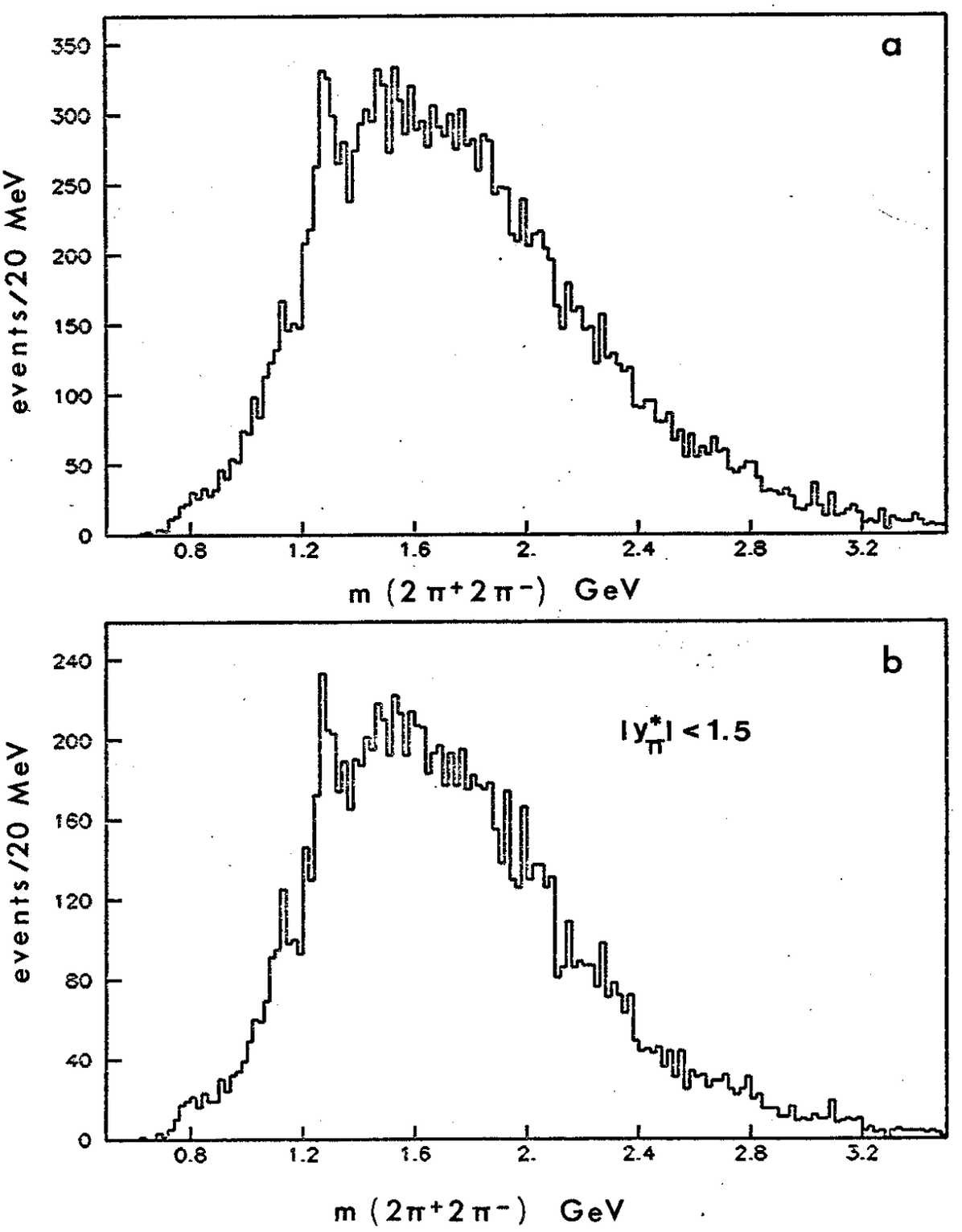
a
events/20 MeV
350
300
250
200
150
100
50
0
0.8
1.2
1.6
2.
2.4
2.8
3.2
m (2π+2π−) GeV
b
$|y^*_\pi| < 1.5$
events/20 MeV
240
200
160
120
80
40
0
0.8
1.2
1.6
2.
2.4
2.8
3.2
m (2π+2π−) GeV

Fig. 21

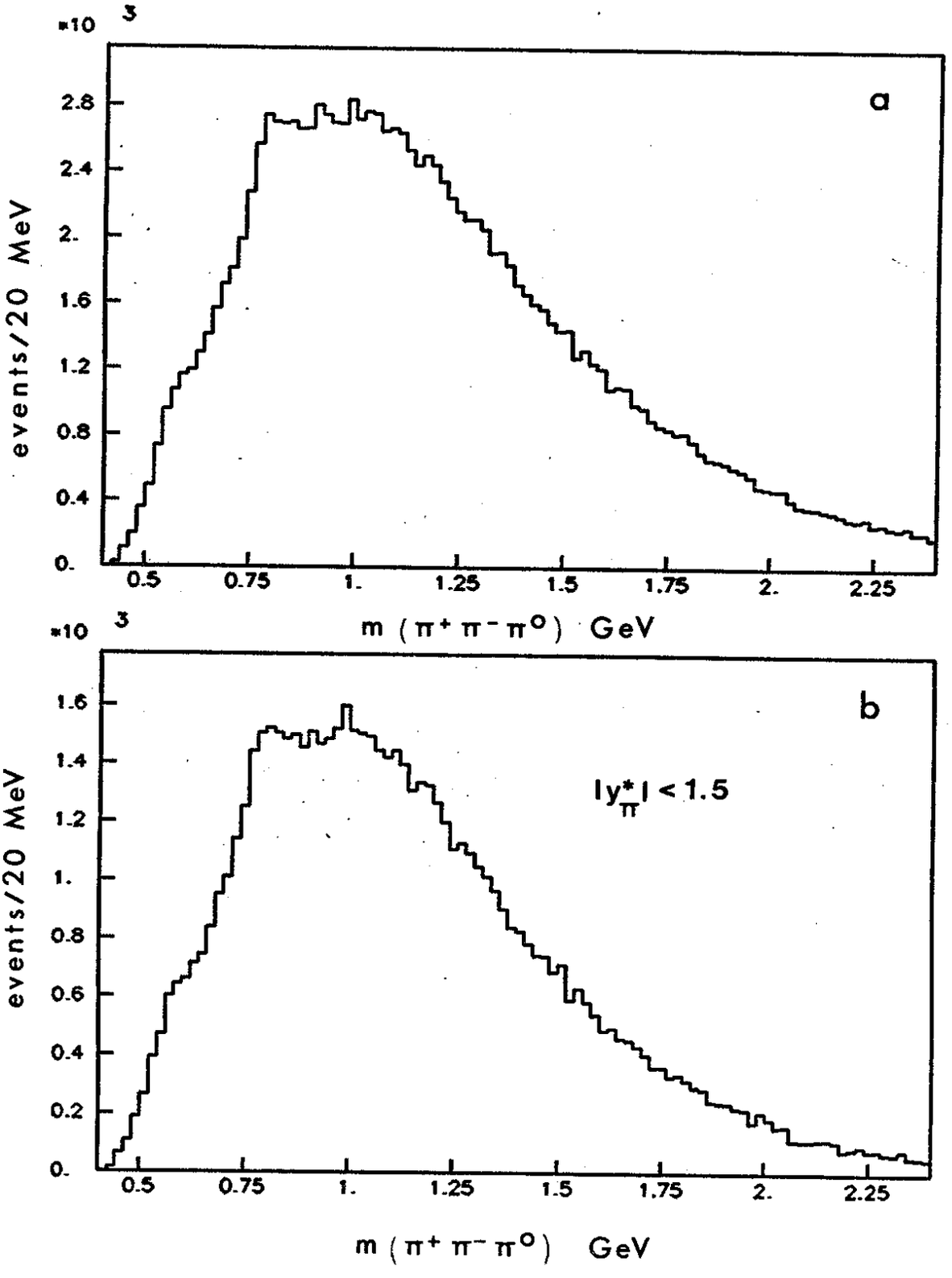
×10 3
2.8
2.4
2.
1.6
1.2
0.8
0.4
0.
events/20 MeV
a
0.5
0.75
1.
1.25
1.5
1.75
2.
2.25
m (π+ π− π°) GeV
×10 3
1.6
1.4
1.2
1.
0.8
0.6
0.4
0.2
0.
events/20 MeV
b
|y*π| < 1.5
0.5
0.75
1.
1.25
1.5
1.75
2.
2.25
m (π+ π− π°) GeV

Fig. 22

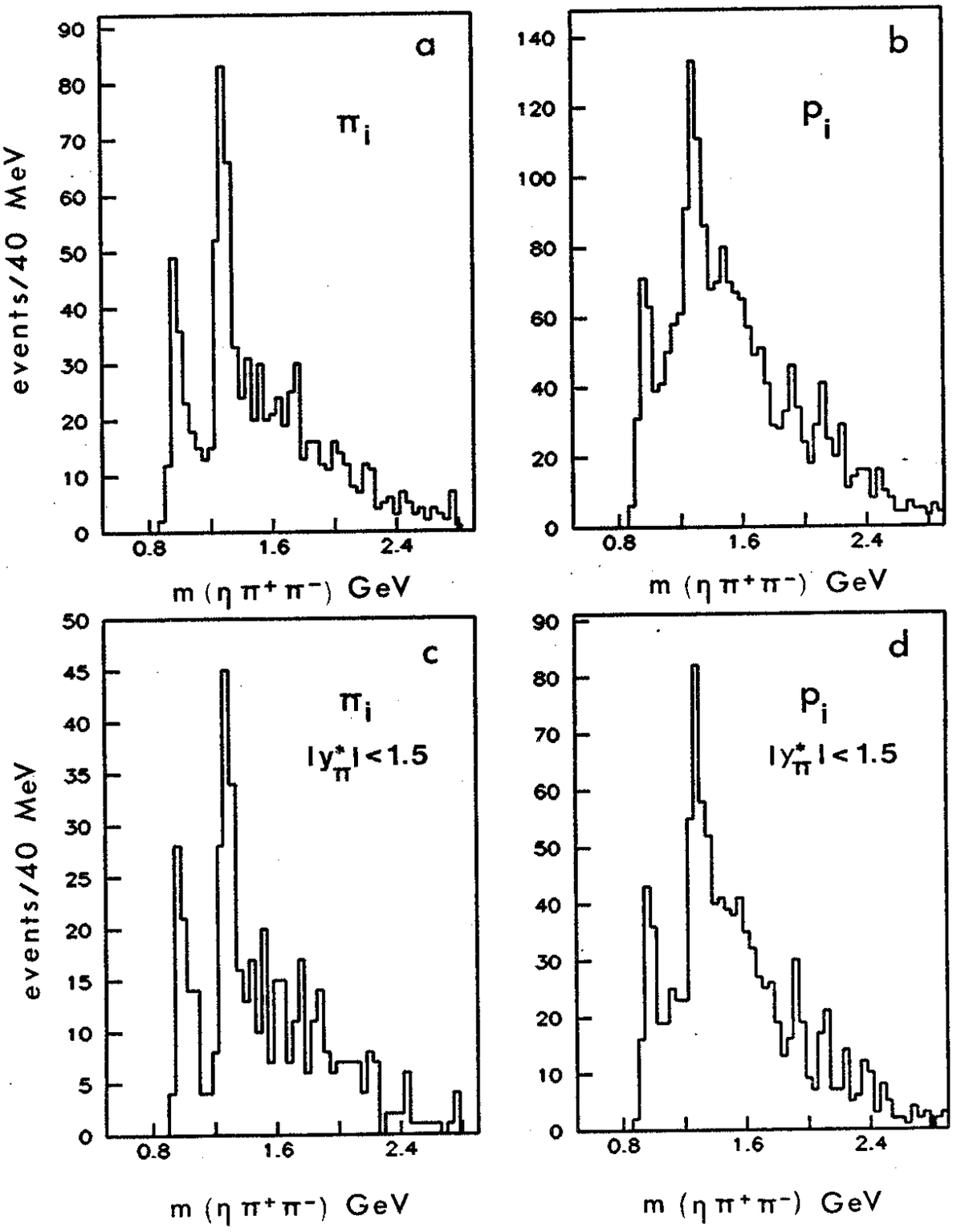
a
π_i
b
p_i
c
π_i
$|y^*_\pi| < 1.5$
d
p_i
$|y^*_\pi| < 1.5$
events/40 MeV
m ($\eta\pi^+\pi^-$) GeV
0.8
1.6
2.4

Fig. 23